Partial State Feedback MRAC based Reconfigurable Fault-Tolerant Control of Drag-Free Satellite with Bounded Estimation Error

Xiaoyun Sun
Shanghai frontiers Science Center of Gravitational Wave Detection, Shanghai Jiaotong University, Shanghai, China

Qiang Shen, Member, IEEE
Shanghai frontiers Science Center of Gravitational Wave Detection, Shanghai Jiaotong University, Shanghai, China

Shufan Wu
Shanghai frontiers Science Center of Gravitational Wave Detection, Shanghai Jiaotong University, Shanghai, China

***Abstract*—Aiming at the ultra-precision and ultra-stable requirements of drag-free control in space detection missions, a multivariable model reference adaptive control (MRAC) scheme is proposed in this paper based on partial observation state, to provide adaptive suppression of uncertain disturbances and improve detection accuracy. The MRAC scheme utilizes model output matching with partial state containing uniform and bounded observation error, and estimates the unknown state parameters through the adaptive law and high-frequency gain decomposition. In response to the actuator bias fault of the drag-free satellite, a set of state error iterative convergence sequence in the actuator loop is established based on the sequence Lyapunov analysis, which is further introduced into the reconfiguration control input to achieve the fault-tolerant target without changing the nominal controller. Through the Lyapunov stability analysis, the convergence of the closed-loop system states in the presence of actuator faults and observation errors is obtained. Numerical simulation results for a 6-DOF drag-free control system demonstrate the effectiveness of the proposed MRAC-based reconfigurable fault-tolerant control scheme.**

***Index Terms*—Partial state feedback; bounded estimation error; multivariable MRAC; drag-free control; reconfigurable control; sequential Lyapunov analysis; fault-tolerant control.**

This work was supported in part by National Key Research and Development Program of the Ministry of Science and Technology of China under Grant 2020YFC2200800, National Natural Science Foundation of China under Grant 62103275 and General project of Shanghai Natural Science Foundation under Grant 20ZR1427000. *(Corresponding author: Shufan Wu)*

Xiaoyun Sun is with the School of Aeronautics and Astronautics, Shanghai Jiaotong University and Shanghai Frontier Science Center for Gravitational Wave Detection, Shanghai, 200240 China (e-mail: sunxiaoyun@sjtu.edu.cn). Shufan Wu is with the School of Aeronautics and Astronautics, Shanghai Jiaotong University and Shanghai Frontier Science Center for Gravitational Wave Detection, Shanghai, 200240 China (e-mail: shufan.wu@sjtu.edu.cn).Qiang Shen is with the School of Aeronautics and Astronautics, Shanghai Jiaotong University and Shanghai Frontier Science Center for Gravitational Wave Detection, Shanghai, 200240 China (e-mail: qiangshen@sjtu.edu.cn).

I. INTRODUCTION

WITH the development of space science and space experiments, such as microgravity science and space-based physics verification, ultra-precision and ultra-stable requirements to dynamic characteristics of orbiting satellite become essential. The drag-free control scheme, utilizing the suspended test masses (TMs) as inertial reference to suppress external disturbances acting on the spacecraft to build an ultra-stable environment of spacecraft platform, has attracted great attention and has been applied in space science experiment satellites such as the Laser Interferometer Space Antenna (LISA) Project [1] .

Currently, the drag-free control can be divided into active control method and passive control method. The passive one is based on closed-loop performance requirements with the attention of the controller robustness to achieve noise suppression. In [2], a frequency domain separation control strategy is proposed based on the full-band demand of the drag-free controller, combined with the mixed sensitivity control scheme, which can realize the separation and decoupling of the control signal and the scientific measurement signal; In [3], combined with quantitative feedback theory, a set of design criteria obtained by the transformation is designed to express the constraints of the SISO controller sensitivity function, adjusting the nominal controller ensuring the boundedness, and meeting different performance specifications. Active methods provide observation feedback of the disturbance or the estimation of the uncertainties, to improve the adaptive stable ability of the system. In [4], a fixed-time controller is designed for the stochastic disturbance to meet the requirements of the low-orbit drag-free satellite. In [5], the embedded model control method (EMC) is adopted, with the expansion observer designed to estimate the external disturbance, the control effect reflects good robustness.

Moreover, to improve the safety and prevent risks, fault detection, diagnosis and fault-tolerant capabilities regarding to actuator faults of the field emission electric propulsion (FEEP) are also considered for the drag-free satellite. In [6], an adaptive fault compensation control scheme is proposed to deal with partial loss of effectiveness and struck of LEO drag-free satellite actuators, and the low-noise requirements are also satisfied when the fault occurs. In [7], aiming at handling multiple faults of the LISA Pathfinder (LPF) spacecraft, the control allocation algorithm (TAA) is designed to realize the model state threshold estimation, and a fault detection, isolation and the reconfigurable control scheme is introduced to achieve the fault-tolerant capability for the drag-free satellite.

In this paper, a fault-tolerant control scheme is developed for drag-free satellite subject to actuator faults and partial state observations. Utilizing the partial observation with uniform and bounded observation error, a model reference adaptive control (MRAC) scheme is designed as baseline drag-free controller. Then, to compensate the 6-DOF actuator faults, a fault-tolerant control (FTC) scheme is proposed using the sequence Lyapunov method. The main contributions of the paper are summarized as follows:

1) A novel fault observer is proposed for actuator bias fault with the utilization of an iterative estimation accuracy predictor, which approximates the steady fault observation error by constructing a uniformly bounded monotonic convergence sequence. The proposed fault observer is convenient to implement on the basis of the existing fault observer in [25], and obtain a much less conservative estimation error bound.
2) Considering the bounded estimation error in the fault observation and partial available state information in practical condition, an extended partial state feedback MRAC scheme is proposed for the drag-free control system to achieve the high-precision control performance. To the best of authors, it is the first time that estimation errors of external disturbances and actuator faults are taken into account in the partial state feedback MRAC scheme when compared with the nominal case in [8], [9], [10], [11], [12], [13], [14], [15], [22], [27], while the boundedness of all closed-loop signals are analyzed theoretically.
3) The steady-state accuracy is firstly discussed and obtained in the practical drag-free control system compared with the previous reports in [2], [3] and [17], which provides a detailed theoretical support to the mission requirement decomposition for drag-free satellite.

The rest of the paper is organized as follows: In Section II, the drag-free control problem is formulated, including space detection satellite drag-free control system and fault actuators modeling. In Section III, the FTC controller is designed in actuator loop with sequential Lyapunov method. In Section IV, the baseline MRAC scheme is designed with partial state and disturbance feedback considering bounded estimation errors, the boundedness of the full closed-loop signals ,the output convergence and stability is proved, the closed-loop accuracy is obtained utilizing the upper bound of the estimation error. In Section V, the simulation environment is introduced to verify the closed-loop state performance and FTC ability of the drag-free controller. Section VI gets the conclusion.

II. PROBLEM FORMULATION

In this section, dynamics of the baseline drag-free satellite and the first-order actuators with bias faults are modeled, then the control problems are formulated with the establishment of the partial state observation MRAC framework, the boundedness assumptions of observation error and uncertainties are given.

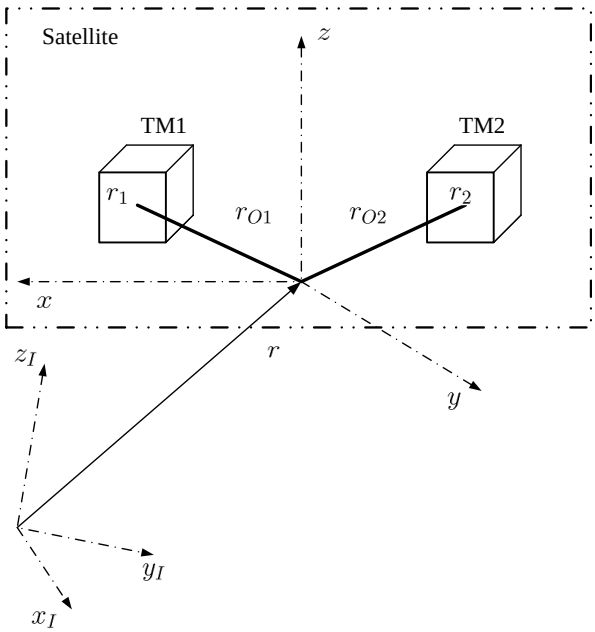

Fig. 1. The 3-body kinematic geometry of drag-free satellite [3].

A. Dynamic Modeling of Drag-free Satellite

Take the LISA Pathfinder gravitational wave detection mission spacecraft as an example in [16], [17], [18] and [19] to model the dynamics of the drag-free control system. The satellite consists of two opposed inertial TMs named TM1 and TM2. The kinematic relationship is shown in the Fig.1.

According to [3], the multi-body dynamics is described as:

$$\begin{pmatrix} \ddot{\boldsymbol{\varphi}} \\ \ddot{\boldsymbol{r}}_{\boldsymbol{1}} \\ \ddot{\boldsymbol{\varphi}}_{\boldsymbol{1}} \\ \ddot{\boldsymbol{r}}_{\boldsymbol{2}} \\ \ddot{\boldsymbol{\varphi}}_{\boldsymbol{2}} \end{pmatrix} = \begin{bmatrix} \boldsymbol{0} & \boldsymbol{I} & \boldsymbol{0} & \boldsymbol{0} & \boldsymbol{0} & \boldsymbol{0} \\ -\boldsymbol{T}_{\boldsymbol{1B}} & \boldsymbol{T}_{\boldsymbol{1B}}\tilde{\boldsymbol{r}}_{\boldsymbol{o1}} & \boldsymbol{I} & \boldsymbol{0} & \boldsymbol{0} & \boldsymbol{0} \\ \boldsymbol{0} & -\boldsymbol{T}_{\boldsymbol{1B}} & \boldsymbol{0} & \boldsymbol{I} & \boldsymbol{0} & \boldsymbol{0} \\ -\boldsymbol{T}_{\boldsymbol{2B}} & \boldsymbol{T}_{\boldsymbol{2B}}\tilde{\boldsymbol{r}}_{\boldsymbol{o2}} & \boldsymbol{0} & \boldsymbol{0} & \boldsymbol{I} & \boldsymbol{0} \\ \boldsymbol{0} & -\boldsymbol{T}_{\boldsymbol{2B}} & \boldsymbol{0} & \boldsymbol{0} & \boldsymbol{0} & \boldsymbol{I} \end{bmatrix} \begin{pmatrix} \boldsymbol{a} \\ \boldsymbol{\alpha} \\ \boldsymbol{a}_{\boldsymbol{1}} \\ \boldsymbol{\alpha}_{\boldsymbol{1}} \\ \boldsymbol{a}_{\boldsymbol{2}} \\ \boldsymbol{\alpha}_{\boldsymbol{2}} \end{pmatrix}, \tag{1}$$

where $\boldsymbol{\varphi}$ is the attitude of the satellite, $\boldsymbol{r}_i$ and $\boldsymbol{\varphi}_i$ are the position and attitude of the two TMs defined as $\boldsymbol{r_i} = [x_i, y_i, z_i]^{\mathrm{T}}$ and $\boldsymbol{\varphi_i} = [\theta_i, \eta_i, \phi_i]^{\mathrm{T}}$ for $i \in \{1, 2\}$, $\boldsymbol{T_{1B}}, \boldsymbol{T_{2B}}$ are the transformation matrices from the satellite to the TMs under the nominal position. $\tilde{\boldsymbol{r}}_{\boldsymbol{o1}}, \tilde{\boldsymbol{r}}_{\boldsymbol{o2}}$ are oblique symmetric cross matrices defined by the nominal position vector $\boldsymbol{r_{o1}} = [r_{o1,x}, r_{o1,y}, r_{o1,z}]^{\mathrm{T}}, \boldsymbol{r_{o2}} = [r_{o2,x}, r_{o2,y}, r_{o2,z}]^{\mathrm{T}}$, expressed as

$$\tilde{\boldsymbol{r}}_{\boldsymbol{o1}} = \begin{bmatrix} 0 & -r_{O1,z} & r_{O1,y} \\ r_{O1,z} & 0 & -r_{O1,x} \\ -r_{O1,y} & r_{O1,x} & 0 \end{bmatrix},$$

$$\tilde{\boldsymbol{r}}_{\boldsymbol{o2}}=\begin{bmatrix}0 & -r_{O2,z} & r_{O2,y}\\ r_{O2,z} & 0 & -r_{O2,x}\\ -r_{O2,y} & r_{O2,x} & 0\end{bmatrix}.$$

Define the acceleration of spacecraft and test masses as

$$\boldsymbol{\alpha}=J^{-1}\boldsymbol{t},\boldsymbol{a}=\frac{1}{m}\boldsymbol{f},\boldsymbol{\alpha_1}=J_1^{-1}\boldsymbol{t_1},$$

$$\boldsymbol{a_1}=\frac{1}{m_1}\boldsymbol{f_1},\boldsymbol{\alpha_2}=J_2^{-1}\boldsymbol{t_2},\boldsymbol{a_2}=\frac{1}{m_2}\boldsymbol{f_2},$$

where m,m_1,m_2,J,J_1,J_2 are masses and inertia moments of satellite and TMs, $\boldsymbol{f},\boldsymbol{f_1},\boldsymbol{f_2},\boldsymbol{t},\boldsymbol{t_1},\boldsymbol{t_2}$ are the combined external forces and moments.

When performing Science Mode 1 (or Test Mode M3), 3 translational DOF, 1 rotational DOF of TM1 and 2 translational DOF of TM2 are selected for drag-free control, and the remaining 6-DOF is performed as suspension control [20]. Define the coordinate selection matrices $\boldsymbol{D_{DF}}$ and $\boldsymbol{D_{SUS}}$ obtained in [21], and rewrite the dynamic model of the drag-free system as:

$$\begin{pmatrix}\ddot{\boldsymbol{\varphi}}\\ \ddot{\boldsymbol{q}}_{\boldsymbol{DF}}\\ \ddot{\boldsymbol{q}}_{\boldsymbol{SUS}}\end{pmatrix}=\begin{bmatrix}\boldsymbol{B_{ATT}} & \boldsymbol{0}\\ \boldsymbol{D_{DF}B_1} & \boldsymbol{D_{DF}B_2}\\ \boldsymbol{D_{SUS}B_1} & \boldsymbol{D_{SUS}B_2}\end{bmatrix}\begin{pmatrix}\boldsymbol{a_{SC}}\\ \boldsymbol{a_{TM}}\end{pmatrix},\quad(2)$$

where $\boldsymbol{q_{DF}},\boldsymbol{q_{SUS}}$ are the drag-free control and electrostatic suspension control coordinates, $\boldsymbol{q_{DF}}=\boldsymbol{D_{DF}q}$, $\boldsymbol{q_{SUS}}=\boldsymbol{D_{SUS}q}$, $\boldsymbol{q}$ is the relative displacement of the TMs, $\boldsymbol{B_1},\boldsymbol{B_2},\boldsymbol{B_{ATT}}$ are parameter matrices, defined as:

$$\boldsymbol{B_{ATT}}=\begin{bmatrix}\boldsymbol{0} & \boldsymbol{I}\end{bmatrix},\boldsymbol{B_1}=\begin{bmatrix}\boldsymbol{-T_{1B}} & \boldsymbol{T_{1B}\tilde{r}_{o1}}\\ \boldsymbol{0} & \boldsymbol{-T_{1B}}\\ \boldsymbol{-T_{2B}} & \boldsymbol{T_{2B}\tilde{r}_{o2}}\\ \boldsymbol{0} & \boldsymbol{-T_{2B}}\end{bmatrix},\boldsymbol{B_2}=\boldsymbol{I},$$

$\boldsymbol{a_{SC}},\boldsymbol{a_{TM}}$ are the combined external forces and moments from the satellite and the TMs, $\boldsymbol{a_{SC}}=\begin{pmatrix}\boldsymbol{a}^{\mathrm{T}} & \boldsymbol{\alpha}^{\mathrm{T}}\end{pmatrix}^{\mathrm{T}},\boldsymbol{a_{TM}}=\begin{pmatrix}\boldsymbol{a_1}^{\mathrm{T}} & \boldsymbol{\alpha_1}^{\mathrm{T}} & \boldsymbol{a_2}^{\mathrm{T}} & \boldsymbol{\alpha_2}^{\mathrm{T}}\end{pmatrix}^{\mathrm{T}}$. It is considered that the actuation external force and moment are composed of controller input $\boldsymbol{u_T},\boldsymbol{u_S}$, external interference $\boldsymbol{d_{SC}},\boldsymbol{d_{TMs}}$ and TM stiffness deformation, expressed as:

$$\boldsymbol{a_{SC}}=\boldsymbol{u_T}+\boldsymbol{d_{SC}},\boldsymbol{a_{TM}}=\boldsymbol{u_S}+\boldsymbol{d_{TMs}}+\begin{bmatrix}\boldsymbol{-\Omega_1^2} & \boldsymbol{0}\\ \boldsymbol{0} & \boldsymbol{-\Omega_2^2}\end{bmatrix}\boldsymbol{q},$$

where $\boldsymbol{\Omega_1},\boldsymbol{\Omega_2}$ are the stiffness matrices. The system open-loop dynamics is finally denoted as:

$$\begin{pmatrix}\ddot{\boldsymbol{\varphi}}\\ \ddot{\boldsymbol{q}}_{\boldsymbol{DF}}\\ \ddot{\boldsymbol{q}}_{\boldsymbol{SUS}}\end{pmatrix}=\begin{bmatrix}\boldsymbol{B_{ATT}} & \boldsymbol{0} & \boldsymbol{0}\\ \boldsymbol{B_{DF}} & \boldsymbol{I} & \boldsymbol{0}\\ \boldsymbol{B_{SUS}} & \boldsymbol{0} & \boldsymbol{I}\end{bmatrix}\left(\begin{pmatrix}\boldsymbol{u_{T_0}}\\ \boldsymbol{u_{S1}}\\ \boldsymbol{u_{S2}}\end{pmatrix}+\begin{pmatrix}\boldsymbol{d_{SC}}\\ \boldsymbol{d_{TM1}}\\ \boldsymbol{d_{TM2}}\end{pmatrix}\right)+\begin{bmatrix}\boldsymbol{0} & \boldsymbol{0} & \boldsymbol{0}\\ \boldsymbol{0} & \boldsymbol{-\Omega_{DF}^2} & \boldsymbol{0}\\ \boldsymbol{0} & \boldsymbol{-\Omega_C^2} & \boldsymbol{-\Omega_{SUS}^2}\end{bmatrix}\begin{pmatrix}\boldsymbol{\varphi}\\ \boldsymbol{q_{DF}}\\ \boldsymbol{q_{SUS}}\end{pmatrix},\quad(3)$$

where, $\boldsymbol{B_{DF}}=\boldsymbol{D_{DF}B_1},\boldsymbol{B_{SUS}}=\boldsymbol{D_{SUS}B_1}$, the controller input $\boldsymbol{u_{S1}}=\boldsymbol{D_{DF}B_2u_S},\boldsymbol{u_{S2}}=\boldsymbol{D_{SUS}B_2u_S}$, the input noise of drag-free system is expressed as

$$\boldsymbol{d_{TM1}}=\boldsymbol{D_{DF}B_2d_{TMs}},\boldsymbol{d_{TM2}}=\boldsymbol{D_{SUS}B_2d_{TMs}}.$$

Two diagonal matrices $\boldsymbol{\Omega_{DF}^2},\boldsymbol{\Omega_{SUS}^2}$ and an additional cross-coupling matrix $\boldsymbol{\Omega_C^2}$ form the coupling stiffness from the drag-free coordinate to the suspension coordinate, which is defined as:

$$\begin{bmatrix}\boldsymbol{-\Omega_{DF}^2} & \boldsymbol{0}\\ \boldsymbol{-\Omega_C^2} & \boldsymbol{-\Omega_{SUS}^2}\end{bmatrix}=\begin{pmatrix}\boldsymbol{D_{DF}}\\ \boldsymbol{D_{SUS}}\end{pmatrix}\begin{bmatrix}\boldsymbol{-\Omega_1^2} & \boldsymbol{0}\\ \boldsymbol{0} & \boldsymbol{-\Omega_2^2}\end{bmatrix}\begin{pmatrix}\boldsymbol{D_{DF}}\\ \boldsymbol{D_{SUS}}\end{pmatrix}^{-1}.$$

Aiming at the analysis of drag-free loop, define the state variable $\boldsymbol{x}=\left[\dot{\boldsymbol{q}}_{\boldsymbol{DF}},\boldsymbol{q_{DF}}\right]^T$. Since the control bandwidth of the TM actuator is much smaller than the FEEP that has realized input decoupling, the control input u_{S1} caused by TM and the disturbance $\boldsymbol{d_{TM1}}$ will unified as the lumped external disturbance, the baseline drag-free dynamic model considering the FEEP input noise is expressed as:

$$\begin{aligned}\dot{\boldsymbol{x}}&=\boldsymbol{A}\boldsymbol{x}+\boldsymbol{B}\left(\boldsymbol{u_T}+\boldsymbol{d_{TM}}\right),\\ \boldsymbol{y}&=\boldsymbol{C}\boldsymbol{x},\end{aligned}\quad(4)$$

where $\boldsymbol{A}=\begin{bmatrix}\boldsymbol{0} & \boldsymbol{I}\\ \boldsymbol{-\Omega_{DF}^2} & \boldsymbol{0}\end{bmatrix},\boldsymbol{B}=\begin{bmatrix}\boldsymbol{0}\\ \boldsymbol{B_{DF}}\end{bmatrix}$ are the state parameter matrices, $\boldsymbol{A},\boldsymbol{B}$ are unknown and slowly time-varying. $\boldsymbol{C}$ is the output parameter matrix, and y is the system output. The total disturbance $\boldsymbol{d_{TM}}=\boldsymbol{B^{-1}}\left(\boldsymbol{u_{S1}}+\boldsymbol{d_{TM1}}\right)+\boldsymbol{d_{SC}}$. $\boldsymbol{d_{TM}}$ is bounded, $\boldsymbol{y}$ defines the system output, and the FEEP actuator inputs $\boldsymbol{u_T}=\boldsymbol{u_{T_0}}+\boldsymbol{d_{SC}}$. The frequency domain description of the drag-free control system (7) is described as:

$$\boldsymbol{y}\left(t\right)=\boldsymbol{G}\left(s\right)\left[\boldsymbol{u}\right]\left(t\right),\boldsymbol{G}\left(s\right)=\boldsymbol{C}(s\boldsymbol{I}-\boldsymbol{A})^{-1}\boldsymbol{B},\quad(5)$$

where $\boldsymbol{u}\left(t\right)=\boldsymbol{u_T}\left(t\right)+\boldsymbol{d_{TM}}\left(t\right)$. For $\boldsymbol{y}\left(t\right)=\boldsymbol{G}\left(s\right)\left[\boldsymbol{u}\right]\left(t\right)$, $[\cdot]$ is a simple symbol that combines time domain and frequency domain signal operations [24].

According to [22] and [24], the following lemma is given:

Lemma 2.1: For any $M\times M$ strictly appropriate and full-rank rational matrix $\boldsymbol{G}\left(s\right)$, there is a lower triangular polynomial matrix $\boldsymbol{\xi_m}\left(s\right)$, defined as the left modified interaction matrix of $\boldsymbol{G}\left(s\right)$, in the form as

$$\boldsymbol{\xi_m}\left(s\right)=\begin{bmatrix}d_1\left(s\right) & 0 & \ldots & \ldots & 0\\ h_{21}^m\left(s\right) & d_2\left(s\right) & 0 & \ldots & 0\\ \vdots & \vdots & \vdots & \vdots & \vdots\\ h_{M1}^m\left(s\right) & \ldots & \ldots & h_{MM-1}^m\left(s\right) & d_M\left(s\right)\end{bmatrix},\quad(6)$$

where $h_{ij}^m\left(s\right),j=1,\ldots,M-1,i=2,\ldots.M$ is a polynomial, and $d_i\left(s\right),i=1,\ldots,M$ is a monotonically stable polynomial of dimension $l_i>0$, such that the high-frequency gain matrix of $\boldsymbol{G}\left(s\right)$ is defined as $\boldsymbol{K_p}=\lim\limits_{s\to\infty}\boldsymbol{\xi_m}\left(s\right)\boldsymbol{G}\left(s\right)$, which is finite and non-singular. Considering partial state with observation errors is introduced to realize feedback control, and the observation output $\hat{\boldsymbol{y}}_{\boldsymbol{0}}$ is expressed as

$$\hat{\boldsymbol{y}}_{\boldsymbol{0}}\left(t\right)=\boldsymbol{C_0}\boldsymbol{x}\left(t\right)+\tilde{\boldsymbol{y}}_{\boldsymbol{0}}\left(t\right)\in\mathbb{R}^{n_0},\quad(7)$$

where $\boldsymbol{C_0}$ is the output selection matrix, $\tilde{\boldsymbol{y}}_{\boldsymbol{0}}$ is the estimation error introduced by uncertainties. Utilizing the estimation output to expand the dimension of required states, so as to realize the design of the full-state feedback controller. The control goal is to construct a feed back control law with the partial state vector $\boldsymbol{y_0}\left(t\right)$ asymptotically tracking the reference vector $\boldsymbol{y_m}\left(t\right)$ generated from

a reference model system $\boldsymbol{y_m}(t) = \boldsymbol{W_m}(s)[\boldsymbol{r}](t)$, where $\boldsymbol{W_m}(s) = \boldsymbol{\xi_m^{-1}}(s)$ is stable and $\boldsymbol{r}(t) \in \mathbb{R}^M$is bounded.

In order to meet the prerequisites of the controller design, the assumptions are shown as follows:

Assumption 2.1: All zero points of $\boldsymbol{G}(s) = \boldsymbol{C}(s\boldsymbol{I} - \boldsymbol{A})^{-1}\boldsymbol{B}$ are stable, and $(\boldsymbol{A}, \boldsymbol{B}, \boldsymbol{C})$ is stable and detectable.

Assumption 2.2: $\boldsymbol{G}(s)$ is full rank and its left modified interaction matrix $\boldsymbol{\xi_m}$ is known.

Assumption 2.3: $\tilde{\boldsymbol{y}}_{\boldsymbol{0}}(t)$ is continuous and bounded, and the upper bound is defined as

$$\lim_{t\to\infty} \sup \|\tilde{\boldsymbol{y}}_{\boldsymbol{0}}(t)\| \le \rho_y, \rho_y \ge 0.$$

Assumption 2.4: Consider that uncertainties of the drag-free dynamics are assumed to be bounded. Then, the disturbed system with uncertainties can be described as:

$$\begin{aligned}\dot{\boldsymbol{x}} &= \boldsymbol{A}_0\boldsymbol{x} + \boldsymbol{\zeta}_1(\boldsymbol{x}, \boldsymbol{u_T}) + \boldsymbol{B}_0(\boldsymbol{u_T} + \boldsymbol{d_{TM}}),\\ \boldsymbol{y} &= \boldsymbol{C}_0\boldsymbol{x} + \boldsymbol{\zeta}_2(\boldsymbol{x}),\end{aligned}$$

where the uncertainties $\boldsymbol{\zeta}_1(\boldsymbol{x}, \boldsymbol{u_T})$ and $\boldsymbol{\zeta}_2(\boldsymbol{x})$ are assumed to be bounded, the nominal system matrices $\boldsymbol{A_0}, \boldsymbol{B_0}, \boldsymbol{C_0}$ are known.

Remark 2.1: The stability of the state parameter matrix $(\boldsymbol{A}, \boldsymbol{B}, \boldsymbol{C})$ and zero points of the tranfer function $\boldsymbol{G}(s)$ is guaranteed by the stiffness matrix $-\boldsymbol{\Omega}_{DF}^2$ in (4). According to [1], [3], for the LISA Pathfinder mission, the stiffness matrix $-\boldsymbol{\Omega}_{DF}^2$ possesses a nominal stable term $-\boldsymbol{\Omega}_{DF0}^2$ with a small perturbation that is approximately $\pm 5\%$ (see detailed values in subsection V.A Parameter Settings), so that **Assumption 2.1** and **Assumption 2.2** hold. In practice, the parameter uncertainties and the measurement errors are bounded, as mentioned in [2], [3], [7], so that the expression in **Assumption 2.3** and **Assumption 2.4** is also reasonable for the practical case.

B. FEEP actuator fault dynamic modeling

Considering the bias fault in the simplified first-order actuator loop, establish the following faulty actuator dynamics:

$$\dot{\boldsymbol{u}}_T = \boldsymbol{\Lambda}(\boldsymbol{u_T} - \boldsymbol{u_c} + \bar{\boldsymbol{u}}), \tag{8}$$

where $\boldsymbol{u_c}$ is the control input, $\bar{\boldsymbol{u}}$ is the performance loss bias, $\bar{\boldsymbol{u}} < 0$, $\|\bar{\boldsymbol{u}}\| \le \rho_b$, $\boldsymbol{\Lambda} < 0$ represents the internal inertia coefficient of the actuator, $||\boldsymbol{\Lambda}|| \gg 1$, and the minimum and maximum characteristic value of $\boldsymbol{\Lambda}^{-1}$ is λ_n and λ_x. Cross-coupling and actuator noise $\boldsymbol{d_{SC}}$ is regarded as external bounded disturbance, so they are no longer reflected in FEEP dynamics.

Generally, the bias $\bar{\boldsymbol{u}}$ is a constant or slowly changing. Take two moments with a very short interval of $T = t_2 - t_1, t_2 > t_1$, the fault dynamics of the actuator is obtained as:

$$\begin{cases}\dot{\boldsymbol{u}}_{\boldsymbol{T_1}} = \boldsymbol{\Lambda}\left(\boldsymbol{u_{T_1}} - \boldsymbol{u_{c_{t_1}}} + \bar{\boldsymbol{u}}_{\boldsymbol{t_1}}\right)\\ \dot{\boldsymbol{u}}_{\boldsymbol{T_2}} = \boldsymbol{\Lambda}\left(\boldsymbol{u_{T_2}} - \boldsymbol{u_{c_{t_2}}} + \bar{\boldsymbol{u}}_{\boldsymbol{t_2}}\right),\end{cases} \tag{9}$$

where, $\boldsymbol{u_{T_1}}, \boldsymbol{u_{T_2}}, \boldsymbol{u_{c_{t_1}}}, \boldsymbol{u_{c_{t_2}}}, \bar{\boldsymbol{u}}_{\boldsymbol{t_1}}, \bar{\boldsymbol{u}}_{\boldsymbol{t_2}}$ correspond to the real input, control input and performance loss bias at the moment t_1, t_2 respectively, and assume $\bar{\boldsymbol{u}}_{\boldsymbol{t_1}} = \bar{\boldsymbol{u}}_{\boldsymbol{t_2}} = \bar{\boldsymbol{u}}$. Subtract the above two equations and get:

$$\dot{\boldsymbol{u}}_{\boldsymbol{T_\delta}} = \boldsymbol{\Lambda}\left(\boldsymbol{u_{T_\delta}} - \boldsymbol{u_{c_T}}\right), \tag{10}$$

where $\boldsymbol{u_{T_\delta}} = \boldsymbol{u_{T_2}} - \boldsymbol{u_{T_1}}, \boldsymbol{u_{c_T}} = \boldsymbol{u_{c_{t_2}}} - \boldsymbol{u_{c_{t_1}}}$. Due to the short time interval T,

$$\boldsymbol{u_{T_\delta}} = T\frac{\boldsymbol{u_{T_2}} - \boldsymbol{u_{T_1}}}{T} \approx T\,\dot{\boldsymbol{u}}_{\boldsymbol{T}}|_{t=t_1} \approx T\dot{\boldsymbol{u}}_{\boldsymbol{T}}, \tag{11}$$

Substituting (11) into (8) and obtain:

$$\begin{cases}\boldsymbol{u_{T_\delta}} = T\dot{\boldsymbol{u}}_{\boldsymbol{T}}\\ \dot{\boldsymbol{u}}_{\boldsymbol{T}} - \dot{\boldsymbol{u}}_{\boldsymbol{T_\delta}} = \boldsymbol{\Lambda}\left(\boldsymbol{u_T} - \boldsymbol{u_{T_\delta}} - (\boldsymbol{u_c} - \boldsymbol{u_{c_T}}) + \bar{\boldsymbol{u}}\right)\end{cases} \tag{12}$$

When the bias faults occur, the following controller form is designed to realize the system retrofit:

$$\boldsymbol{u_c} = \boldsymbol{u_T} + \boldsymbol{u_r}, \tag{13}$$

where the retrofit control input $\boldsymbol{u_r} = -\hat{\bar{\boldsymbol{u}}}$, $\hat{\bar{\boldsymbol{u}}}$ is the performance loss bias estimation obtained by state observer.

Remark 2.2: In the faulty actuator dynamics (8), the performance loss bias fault $\bar{\boldsymbol{u}}$ modeled in [6] is considered. According to [6], among the various fault types of the FEEP actuators (Micro-Newton Thrusters), the performance loss bias fault is one of the most commonly occurring faults due to the circuit failure of the electronic actuation. In addition, the performance loss bias fault is also widely discussed in the satellite control engineering, as reported in [8], [10], [12], [13].

C. Control Problem Formulation

Reconfigurable FTC problem of the drag-free control system under actuator faults. According to the controller framework given in (13), the reconfiguration control input u_r is applied to compensate the state change caused by the actuator faults. To improve compensation accuracy, the fault estimation needs higher precision compared with conventional solutions [13]. When designing the fault observer, Lyapunov analysis is introduced to construct a unified and bounded monotonic convergence sequence, which converts the reconfigurable control problem into an iterative approximation fault estimation problem.

The precise control problem of drag-free satellite via partial observation state feedback with estimation error. In the LISA Pathfinder detection mission, the following performance requirements of the residual acceleration in the direction of the sensitive axis is shown as follows [16]:

$$S_a^{1/2}(f) \le 3\times 10^{-14}\left[1 + \left(\frac{f}{3mHz}\right)^2\right] m/s^2/\sqrt{Hz}, \tag{14}$$

where, $S_a^{1/2}(f)$ is the spectral density of the residual acceleration in the direction of the sensitive axis, which indicates that in the drag-free control problem, each channel needs extremely high precision when dealing with uncertainties and complex external disturbance. Discuss the condition that partial states are lost and there are bounded estimation errors in the known states. Only known states

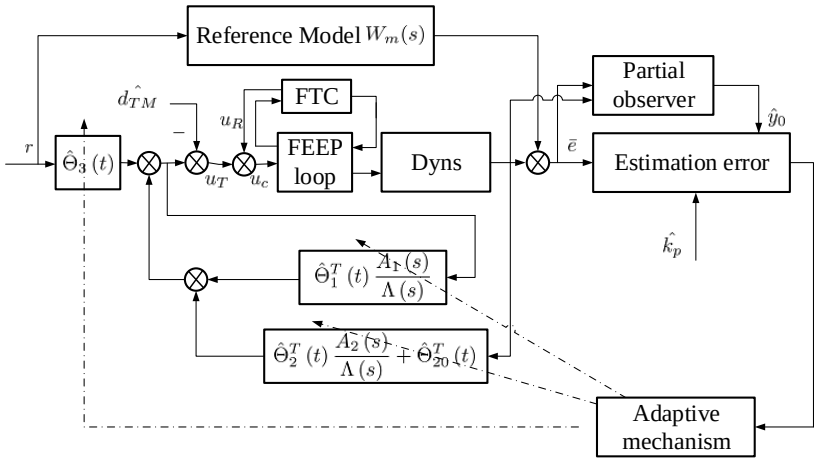

Fig. 2. Control framework.

are used to design the feedback controller, and the MRAC scheme is applied to achieve the approximation of all channels to the reference model, which is used to achieve nonlinear suppression and improve system stability. The control framework is shown in Fig.2.

III. RECONFIGURABLE FAULT-TOLERANT CONTROLLER DESIGN

To approximate the actuators faults, the state observer is firstly designed as follows:

$$\begin{cases} \boldsymbol{\Lambda}^{-1}\left(\dot{\hat{\boldsymbol{u}}}_{\boldsymbol{T\delta}}-\dot{\hat{\boldsymbol{u}}}_{\boldsymbol{T}}\right)=\hat{\boldsymbol{u}}_{\boldsymbol{T\delta}}-\hat{\boldsymbol{u}}_{\boldsymbol{T}}+\left(\boldsymbol{u_c}-\boldsymbol{u_{cT}}\right) \\ -\boldsymbol{l_1}\left(\boldsymbol{u}_{\boldsymbol{T\delta}}-\hat{\boldsymbol{u}}_{\boldsymbol{T\delta}}+\boldsymbol{k_1}\left(\boldsymbol{u_T}-\hat{\boldsymbol{u}}_{\boldsymbol{T}}\right)\right) \\ \hat{\boldsymbol{u}}_{\boldsymbol{T\delta}}=T\dot{\hat{\boldsymbol{u}}}_{\boldsymbol{T}} \end{cases}, \quad (15)$$

where $\hat{\boldsymbol{u}}_{\boldsymbol{T}}, \hat{\boldsymbol{u}}_{\boldsymbol{T\delta}}$ are the state estimations obtained by the observer, $\boldsymbol{l_1}, \boldsymbol{k_1}$ are the observer gains, which satisfy $\boldsymbol{k_1}=\boldsymbol{k_1}^{\mathrm{T}}>0, \boldsymbol{l_1}-\boldsymbol{I}>0$. Let the state estimation error $\tilde{\boldsymbol{u}}_{\boldsymbol{T\delta}}=\boldsymbol{u}_{\boldsymbol{T\delta}}-\hat{\boldsymbol{u}}_{\boldsymbol{T\delta}}, \tilde{\boldsymbol{u}}_{\boldsymbol{T}}=\boldsymbol{u_T}-\hat{\boldsymbol{u}}_{\boldsymbol{T}}$, the observation error equation is denoted as:

$$\boldsymbol{\Lambda}^{-1}\left(\dot{\tilde{\boldsymbol{u}}}_{\boldsymbol{T\delta}}-\dot{\tilde{\boldsymbol{u}}}_{\boldsymbol{T}}\right)=\left(\tilde{\boldsymbol{u}}_{\boldsymbol{T\delta}}-\tilde{\boldsymbol{u}}_{\boldsymbol{T}}\right)-\bar{\boldsymbol{u}}-\boldsymbol{l_1}\left(\tilde{\boldsymbol{u}}_{\boldsymbol{T\delta}}+\boldsymbol{k_1}\tilde{\boldsymbol{u}}_{\boldsymbol{T}}\right). \quad (16)$$

Let $\boldsymbol{S}=\tilde{\boldsymbol{u}}_{\boldsymbol{T\delta}}+\boldsymbol{K}\tilde{\boldsymbol{u}}_{\boldsymbol{T}}$, $\boldsymbol{K}=\left(\boldsymbol{l_1}-\boldsymbol{I}\right)^{-1}\left(\boldsymbol{l_1}\boldsymbol{k_1}+\boldsymbol{I}\right)$, it can be obtained that $\boldsymbol{K}=\boldsymbol{K}^{\mathrm{T}}>0$. Utilizing $\hat{\boldsymbol{u}}_{\boldsymbol{T\delta}}=T\dot{\hat{\boldsymbol{u}}}_{\boldsymbol{T}}$ to rewrite the above equation as

$$\boldsymbol{\Lambda}^{-1}\dot{\boldsymbol{S}}=-\bar{\boldsymbol{u}}-\left(\boldsymbol{l_1}-\boldsymbol{I}\right)\boldsymbol{S}+\frac{1}{T}\left(\boldsymbol{K}+\boldsymbol{\Lambda}^{-1}\right)\tilde{\boldsymbol{u}}_{\boldsymbol{T\delta}}. \quad (17)$$

The lemma is shown as:

Lemma 3.1 [15]: Consider that $\boldsymbol{S}=\tilde{\boldsymbol{u}}_{\boldsymbol{T\delta}}+\boldsymbol{K}\tilde{\boldsymbol{u}}_{\boldsymbol{T}}$, if it exists $\bar{\boldsymbol{S}}>0$ and limited time $T>0$, $\|\boldsymbol{S}(t)\|\leq\bar{S}_t$, then

$$\lim_{t\to\infty}\sup\|\tilde{\boldsymbol{u}}_{\boldsymbol{T\delta}}\|\leq\left(\frac{\lambda_{\max}\left(\boldsymbol{K}\right)}{\lambda_{\min}\left(\boldsymbol{K}\right)}+1\right)\bar{S}_t.$$

Then the following theorem is given:

Theorem 3.1: The upper bound of the estimation error $\|\boldsymbol{S}(t)\|$, $\|\tilde{\boldsymbol{u}}_{\boldsymbol{T\delta}}(t)\|$ will finally converge after the i-th iteration:

$$\begin{cases} \lim\limits_{t\to\infty}\sup\|\boldsymbol{S}(t)\|=\bar{S}_i\leq\bar{S}_{i+1}=\sqrt{\dfrac{\lambda_x}{\lambda_n}}\dfrac{\phi\left(\bar{\tilde{u}}_{T_{\delta_i}}\right)}{\lambda_{\min}\left(\boldsymbol{l_1}-\boldsymbol{I}\right)} \\ \lim\limits_{t\to\infty}\sup\|\tilde{\boldsymbol{u}}_{\boldsymbol{T\delta}}(t)\|\leq\left(\dfrac{\lambda_{\max}\left(\left(\boldsymbol{l_1}-\boldsymbol{I}\right)^{-1}\left(\boldsymbol{l_1}\boldsymbol{k_1}+\boldsymbol{I}\right)\right)}{\lambda_{\min}\left(\left(\boldsymbol{l_1}-\boldsymbol{I}\right)^{-1}\left(\boldsymbol{l_1}\boldsymbol{k_1}+\boldsymbol{I}\right)\right)}\right. \\ \left.+1\right)\bar{S}_{i+1}=\bar{\tilde{u}}_{T_{\delta_{i+1}}} \end{cases}, \quad (18)$$

where, $\bar{S}_i, \bar{S}_{i+1}, \bar{\tilde{u}}_{T_{\delta_i}}, \bar{\tilde{u}}_{T_{\delta_{i+1}}}$ are the upper bounds of the estimation error after iteration, $\lambda_{\max}(\boldsymbol{k})$, $\lambda_{\min}(\boldsymbol{k})$ are the maximum or minimum eigenvalue of matrix $\boldsymbol{k}$, and $\phi\left(\bar{\tilde{u}}_{T_{\delta_i}}\right)$ is the monotonically increasing function defined by (21), Both $\left\{\bar{S}_i\right\}_{i\in\mathbb{Z}^+}, \left\{\bar{\tilde{u}}_{T_{\delta_i}}\right\}_{i\in\mathbb{Z}^+}$ are strictly decreasing convergence sequences. The fault observation can be calculated by the estimation upper bound and obtained as follows:

$$\begin{aligned} \hat{\bar{\boldsymbol{u}}}=&-\left(\boldsymbol{l_1}-\boldsymbol{I}\right)\left(\boldsymbol{l_1}\boldsymbol{k_1}+\boldsymbol{I}\right)^{-1}\boldsymbol{l_1}\boldsymbol{k_1}\bar{S}_{i+1} \\ &+\left(\left(\boldsymbol{l_1}-\boldsymbol{I}\right)\left(\boldsymbol{l_1}\boldsymbol{k_1}+\boldsymbol{I}\right)^{-1}\boldsymbol{l_1}\boldsymbol{k_1}-\boldsymbol{l_1}\right)\bar{\tilde{u}}_{T_{\delta_{i+1}}}. \end{aligned} \quad (19)$$

Proof: The Lyapunov function is given as:

$$V_0=\frac{1}{2}\boldsymbol{S}^{\mathrm{T}}\boldsymbol{\Lambda}^{-1}\boldsymbol{S}. \quad (20)$$

Differentiate the above equation and yield:

$$\begin{aligned} \dot{V}_0&=\boldsymbol{S}^{\mathrm{T}}\boldsymbol{\Lambda}^{-1}\dot{\boldsymbol{S}} \\ &\leq\|\boldsymbol{S}\|\left(-\lambda_{\min}\left(\boldsymbol{l_1}-\boldsymbol{I}\right)\|\boldsymbol{S}\|+\|\bar{\boldsymbol{u}}\|\right. \\ &+\frac{1}{T}\left(\left(\boldsymbol{l_1}-\boldsymbol{I}\right)^{-1}\left(\boldsymbol{l_1}\boldsymbol{k_1}+\boldsymbol{I}\right)+\boldsymbol{\Lambda}^{-1}\right)\|\tilde{\boldsymbol{u}}_{\boldsymbol{T\delta}}\|\Big) \\ &\leq-\lambda_{\min}\left(\boldsymbol{l_1}-\boldsymbol{I}\right)\|\boldsymbol{S}\|^2+\left(\|\bar{\boldsymbol{u}}\|\right. \\ &+\frac{1}{T}\left(\left(\boldsymbol{l_1}-\boldsymbol{I}\right)^{-1}\left(\boldsymbol{l_1}\boldsymbol{k_1}+\boldsymbol{I}\right)+\boldsymbol{\Lambda}^{-1}\right)\|\tilde{\boldsymbol{u}}_{\boldsymbol{T\delta}}\|\Big)\|\boldsymbol{S}\| \end{aligned}. \quad (21)$$

Let $\phi\left(\|\tilde{\boldsymbol{u}}_{\boldsymbol{T\delta}}\|\right)=\rho_b+\frac{1}{T}\left(\left(\boldsymbol{l_1}-\boldsymbol{I}\right)^{-1}\left(\boldsymbol{l_1}\boldsymbol{k_1}+\boldsymbol{I}\right)+\boldsymbol{\Lambda}^{-1}\right)\|\tilde{\boldsymbol{u}}_{T_\delta}\|$, it is known that $\phi(\boldsymbol{.})$ is strictly monotonically increasing. Note that

$$\lambda_n\|\boldsymbol{S}\|^2\leq 2V_0\leq\lambda_x\|\boldsymbol{S}\|^2 \quad (22)$$

(21) can be further derived as

$$\dot{V}_0 \leq -\|\boldsymbol{S}\| \left(\lambda_{\min}\left(\boldsymbol{l_1}-\boldsymbol{I}\right) \sqrt{\frac{2V_0}{\lambda_x}} - \phi\left(\|\tilde{\boldsymbol{u}}_{\boldsymbol{T_\delta}}\|\right) \right). \quad (23)$$

Since $\lambda_{\min}\left(\boldsymbol{l_1}-\boldsymbol{I}\right) > 0$ and $\frac{1}{T}((\boldsymbol{l_1}-\boldsymbol{I})^{-1}(\boldsymbol{l_1 k_1}+\boldsymbol{I})+\boldsymbol{\Lambda}^{-1}) > 0$, and it is known that $\phi(\boldsymbol{.})$ strictly increases monotonically, then assume that $\|\tilde{\boldsymbol{u}}_{\boldsymbol{T_\delta}}\|$ bounded, expressed as $\|\tilde{\boldsymbol{u}}_{\boldsymbol{T_\delta}}\| \leq \bar{\tilde{u}}_{T_{\delta_0}} \leq u^*_{T_\delta}$. Note that when $\sqrt{2V_0} > \frac{\sqrt{\lambda_x}\phi\left(\bar{\tilde{u}}_{T_{\delta_0}}\right)}{\lambda_{\min}(\boldsymbol{l_1}-\boldsymbol{I})}$, $\dot{V}_0 < 0$, it can be obtained

$$\begin{aligned} \lim_{t\to\infty} \sup \|\boldsymbol{S}(t)\| &\leq \lim_{t\to\infty} \sup \sqrt{\frac{2V_0(t)}{\lambda_n}} \\ &\leq \bar{S}_1 = \sqrt{\frac{\lambda_x}{\lambda_n}} \frac{\phi\left(\bar{\tilde{u}}_{T_{\delta_0}}\right)}{\lambda_{\min}\left(\boldsymbol{l_1}-\boldsymbol{I}\right)} \end{aligned}. \quad (24)$$

According to the derivation of **Lemma 3.1** and (24), the following set of monotonic inequalities can be obtained:

$$\begin{cases} \lim_{t\to\infty} \sup \|\boldsymbol{S}(t)\| = \bar{S}_0 \leq \bar{S}_1 = \sqrt{\frac{\lambda_x}{\lambda_n}} \frac{\phi\left(\bar{\tilde{u}}_{T_{\delta_0}}\right)}{\lambda_{\min}\left(\boldsymbol{l_1}-\boldsymbol{I}\right)} \\ \lim_{t\to\infty} \sup \|\tilde{\boldsymbol{u}}_{\boldsymbol{T_\delta}}(t)\| \\ \leq \left(\frac{\lambda_{\max}\left((\boldsymbol{l_1}-\boldsymbol{I})^{-1}(\boldsymbol{l_1 k_1}+\boldsymbol{I})\right)}{\lambda_{\min}\left((\boldsymbol{l_1}-\boldsymbol{I})^{-1}(\boldsymbol{l_1 k_1}+\boldsymbol{I})\right)} + 1 \right) \bar{S}_1 = \bar{\tilde{u}}_{T_{\delta_1}} \end{cases}, \quad (25)$$

where, $\bar{S}_1, \bar{\tilde{u}}_{T_{\delta_1}}$ are the actuator state estimation error prediction value obtained based on the first iteration of the monotonic inequalities under the initial state $\bar{S}_0, \bar{\tilde{u}}_{T_{\delta_0}}$. By analogy, after i-th iteration of the above monotonic inequality set, it can be denoted as (18). To formulate the observation procedure, the iterative procedure is given in the following **Algorithm 3.1**:

Algorithm 3.1: $\bar{S}_{i+1}$ can be obtained by the following algorithm:

step 1: Select the initial estimation value $\hat{\boldsymbol{u}}_{\boldsymbol{T_{\delta_0}}}$ and caulculate $\bar{\tilde{u}}_{T_{\delta_0}}$ by $\bar{\tilde{u}}_{T_{\delta_0}} = \left\|\boldsymbol{u}_{\boldsymbol{T_\delta}} - \hat{\boldsymbol{u}}_{\boldsymbol{T_{\delta_0}}}\right\|$.

step 2: Calculate $\bar{S}_1$ by $\bar{S}_1 = \sqrt{\frac{\lambda_x}{\lambda_n}} \frac{\phi\left(\bar{\tilde{u}}_{T_{\delta_0}}\right)}{\lambda_{\min}(\boldsymbol{l_1}-\boldsymbol{I})}$ and continue to *step 3*.

step 3: Calculate $\bar{\tilde{u}}_{T_{\delta_1}}$ by $\bar{\tilde{u}}_{T_{\delta_1}} = \left(\frac{\lambda_{\max}\left((\boldsymbol{l_1}-\boldsymbol{I})^{-1}(\boldsymbol{l_1 k_1}+\boldsymbol{I})\right)}{\lambda_{\min}\left((\boldsymbol{l_1}-\boldsymbol{I})^{-1}(\boldsymbol{l_1 k_1}+\boldsymbol{I})\right)} + 1 \right) \bar{S}_1$ and return to *step 2*, the iteration is completed once.

step 4: Repeating i times of *step 2* and *step 3*, $\bar{\tilde{u}}_{T_{\delta_{i+1}}}$ and $\bar{S}_{i+1}$ are obtained to calculate $\hat{\tilde{\boldsymbol{u}}}$ and $\boldsymbol{u_r}$.

Note the monotonic convergence of the inequalities, two sets of sequences with monotonically decreasing state estimation errors can be obtained as $\left\{\bar{S}_i\right\}_{i\in\mathbb{Z}^+}, \left\{\bar{\tilde{u}}_{T_{\delta_i}}\right\}_{i\in\mathbb{Z}^+}$. Utilizing the sequence Lyapunov scheme to perform i-th iterations on the dynamic state of the actuators, the fault observation is denoted as:

$$\begin{aligned} \boldsymbol{u_r} &= -\hat{\tilde{\boldsymbol{u}}} = \left(\boldsymbol{l_1}-\boldsymbol{I}\right)\left(\boldsymbol{l_1 k_1}+\boldsymbol{I}\right)^{-1}\boldsymbol{l_1 k_1}\bar{S}_{i+1} \\ &- \left(\left(\boldsymbol{l_1}-\boldsymbol{I}\right)\left(\boldsymbol{l_1 k_1}+\boldsymbol{I}\right)^{-1}\boldsymbol{l_1 k_1} - \boldsymbol{l_1}\right)\bar{\tilde{u}}_{T_{\delta_{i+1}}}. \end{aligned} \quad (26)$$

The reconfigurable controller to compensate bias fault will bring the following bounded input errors $\tilde{\boldsymbol{u}}_{\boldsymbol{r}}$ with the following convergence bound:

$$\lim_{t\to\infty} \sup \|\tilde{\boldsymbol{u}}_{\boldsymbol{r}}\| \leq \rho_r. \quad (27)$$

Remark 3.1: In this work, different initial values of $\hat{\boldsymbol{u}}_{\boldsymbol{T_{\delta_0}}}$ are chosen for the healthy case (i.e., the process before fault is detected) and faulty case (i.e., the process after fault is detected). Specifically, initial value of $\hat{\boldsymbol{u}}_{\boldsymbol{T_{\delta_0}}}$ is set to 0 in the healthy case and a calculated value in faulty case, respectively. Inspired by reference [8] of the revised manuscript, the fault detection scheme can also be established as equation (15). The details for choosing the initial value of $\hat{\boldsymbol{u}}_{\boldsymbol{T_{\delta_0}}}$ under the two cases are given as follows:

Case 1: In the healthy case, the initial value of $\hat{\boldsymbol{u}}_{\boldsymbol{T_{\delta_0}}}$ is set to be 0. In this work, since the drag-free control problem in the science mode is discussed, there is no parameter perturbation, and the initial value of $\hat{\boldsymbol{u}}_{\boldsymbol{T_{\delta_0}}}$ can be set to be 0 at the starting of the simulation. Note that in the healthy case, $\|\bar{\boldsymbol{u}}\| = 0$. By using the fault detection scheme in equation (15), the derivative of $\dot{V}_0$ in (21) can be rewritten as:

$$\begin{aligned} \dot{V}_0 &\leq -\lambda_{\min}\left(\boldsymbol{l_1}-\boldsymbol{I}\right)\|\boldsymbol{S}\|^2 \\ &+ \frac{1}{T}\left(\left\|\left(\boldsymbol{l_1}-\boldsymbol{I}\right)^{-1}\left(\boldsymbol{l_1 k_1}+\boldsymbol{I}\right)\right\| + \lambda_x\right)\|\tilde{\boldsymbol{u}}_{\boldsymbol{T_\delta}}\|\,\|\boldsymbol{S}\|. \end{aligned}$$

It is clear that $\dot{V}_0 < 0$ if $\|\boldsymbol{S}\| > \frac{\left(\left\|(\boldsymbol{l_1}-\boldsymbol{I})^{-1}(\boldsymbol{l_1 k_1}+\boldsymbol{I})\right\|+\lambda_x\right)\|\tilde{\boldsymbol{u}}_{\boldsymbol{T_\delta}}\|}{T\lambda_{\min}(\boldsymbol{l_1}-\boldsymbol{I})}$. Therefore the state estimation error $\|\boldsymbol{S}\|$ should always satisfy $\|\boldsymbol{S}\| \leq \frac{\left(\left\|(\boldsymbol{l_1}-\boldsymbol{I})^{-1}(\boldsymbol{l_1 k_1}+\boldsymbol{I})\right\|+\lambda_x\right)\|\tilde{\boldsymbol{u}}_{\boldsymbol{T_\delta}}\|}{T\lambda_{\min}(\boldsymbol{l_1}-\boldsymbol{I})}$ in the healthy case. Otherwise, the fault is detected.

Case 2: In the faulty case (i.e., after the fault is detected), the initial value of $\hat{\boldsymbol{u}}_{\boldsymbol{T_{\delta_0}}}$ is set to $\hat{\boldsymbol{u}}_{\boldsymbol{T_{\delta_0}}} = \hat{\boldsymbol{u}}_{\boldsymbol{T_\delta}}(t)|_{t=T_d}$, where T_d is the time instant that fault is detected. As derived in *Case 1*, the time instant T_d can be obtained once $\|\boldsymbol{S}\| > \frac{\left(\left\|(\boldsymbol{l_1}-\boldsymbol{I})^{-1}(\boldsymbol{l_1 k_1}+\boldsymbol{I})\right\|+\lambda_x\right)\|\tilde{\boldsymbol{u}}_{\boldsymbol{T_\delta}}\|}{T\lambda_{\min}(\boldsymbol{l_1}-\boldsymbol{I})}$.

IV. PARTIAL MRAC DESIGN WITH BOUNDED ESTIMATION ERROR

In this section, a nominal state feedback MRAC scheme is constructed with the model output matching relationship demonstrated, then the stability analysis is shown with the obtain of convergence upper bound considering the bounded estimation error of each state.

A. Baseline Control Framework

Utilizing the known partial state information $\hat{\boldsymbol{y}}_{\boldsymbol{0}}(t) = \boldsymbol{C_0}\hat{\boldsymbol{x}}(t)$ to further realize the observation of the remaining unknown states, and design the baseline state feedback control framework according to the observation state. The baseline control law is expressed as:

$$\boldsymbol{u_T}(t) = \boldsymbol{K_1^{*T}}\hat{\boldsymbol{x}}(t) + \boldsymbol{K_2^*}\boldsymbol{r}(t) - \hat{\boldsymbol{d}}_{\boldsymbol{TM}}, \quad (28)$$

where $\boldsymbol{K_1^*}, \boldsymbol{K_2^*}$ are the feedback gains of the observation state $\hat{\boldsymbol{x}}(t)$ and the reference model input $\boldsymbol{r}(t)$. $\boldsymbol{d_{TM}}$

is supressed by the feedback of $\hat{\boldsymbol{d}}_{\boldsymbol{TM}}$, where $\hat{\boldsymbol{d}}_{\boldsymbol{TM}}$ is obtained by the following observer according to [26]:

$$\dot{\hat{\boldsymbol{d}}}_{\boldsymbol{TM}} = -\boldsymbol{\lambda}\left(\dot{\hat{\boldsymbol{x}}} - \boldsymbol{A_0}\hat{\boldsymbol{x}} - \boldsymbol{B_0}\boldsymbol{u_T} - \hat{\boldsymbol{d}}_{\boldsymbol{TM}}\right),$$

where $\boldsymbol{\lambda} > 0$ is an coefficient to be set. The following assumption is given:

Assumption 4.1: Let the observation error $\tilde{\boldsymbol{d}}_{\boldsymbol{TM}} = \boldsymbol{d}_{\boldsymbol{TM}} - \hat{\boldsymbol{d}}_{\boldsymbol{TM}}$, according to **Assumption 2.4** and [22], $\tilde{\boldsymbol{d}}_{\boldsymbol{TM}}$ is continuous and bounded, and the upper bound is defined as

$$\lim_{t\to\infty}\sup\left\|\tilde{\boldsymbol{d}}_{\boldsymbol{TM}}\right\| \le \rho_d, \rho_d \ge 0.$$

To achieve model output matching and controller construction, partial state observation $\hat{\boldsymbol{y}}_{\boldsymbol{0}}(t)$ is computed to realize the observation of the full state information. Introducing the transformation matrix $\boldsymbol{P} \in \mathbb{R}^{n\times n}$, then $\boldsymbol{C_0}\boldsymbol{P}^{-1} = \begin{bmatrix}\boldsymbol{I_{n_0}} & \boldsymbol{0}\end{bmatrix}$ and $n_0 = rank[\boldsymbol{C_0}]$, the system state equation is converted to $\dot{\bar{\boldsymbol{x}}}(t) = \bar{\boldsymbol{A}}\bar{\boldsymbol{x}}(t) + \bar{\boldsymbol{B}}\boldsymbol{u}(t)$,$\bar{\boldsymbol{A}} = \boldsymbol{PAP}^{-1}$, $\bar{\boldsymbol{B}} = \boldsymbol{PB}$. Express the system full state equation as:

$$\begin{bmatrix}\dot{\bar{\boldsymbol{x}}}_{\boldsymbol{1}}(t)\\ \dot{\bar{\boldsymbol{x}}}_{\boldsymbol{2}}(t)\end{bmatrix} = \begin{bmatrix}\bar{\boldsymbol{A}}_{\boldsymbol{11}} & \bar{\boldsymbol{A}}_{\boldsymbol{12}}\\ \bar{\boldsymbol{A}}_{\boldsymbol{21}} & \bar{\boldsymbol{A}}_{\boldsymbol{22}}\end{bmatrix}\begin{bmatrix}\bar{\boldsymbol{x}}_{\boldsymbol{1}}(t)\\ \bar{\boldsymbol{x}}_{\boldsymbol{2}}(t)\end{bmatrix} + \begin{bmatrix}\bar{\boldsymbol{B}}_{\boldsymbol{1}}\\ \bar{\boldsymbol{B}}_{\boldsymbol{2}}\end{bmatrix}\left(\boldsymbol{u_T}(t) + \boldsymbol{d}_{\boldsymbol{TM}}\right), \tag{29}$$

where $\bar{\boldsymbol{x}}(t) = \boldsymbol{P}\boldsymbol{x}(t) = \left[\bar{\boldsymbol{x}}_{\boldsymbol{1}}{}^{\mathrm{T}}(t) \quad \bar{\boldsymbol{x}}_{\boldsymbol{2}}{}^{\mathrm{T}}(t)\right]^{\mathrm{T}}$,$\bar{\boldsymbol{x}}_{\boldsymbol{1}}(t) \in \mathbb{R}^{n_0}$, $\bar{\boldsymbol{x}}_{\boldsymbol{2}}(t) \in \mathbb{R}^{n-n_0}$, $\bar{\boldsymbol{A}}_{\boldsymbol{11}} \in \mathbb{R}^{n_0\times n_0}$, $\bar{\boldsymbol{A}}_{\boldsymbol{12}} \in \mathbb{R}^{n_0\times(n-n_0)}$,$\bar{\boldsymbol{A}}_{\boldsymbol{21}} \in \mathbb{R}^{(n-n_0)\times n_0}$, $\bar{\boldsymbol{A}}_{\boldsymbol{22}} \in \mathbb{R}^{(n-n_0)\times(n-n_0)}$, $\bar{\boldsymbol{B}}_{\boldsymbol{1}} \in \mathbb{R}^{n_0\times M}$, $\bar{\boldsymbol{B}}_{\boldsymbol{2}} \in \mathbb{R}^{(n-n_0)\times M}$. When $(\boldsymbol{A}, \boldsymbol{C_0})$ is observable and detectable, $\left(\bar{\boldsymbol{A}}_{\boldsymbol{22}}, \bar{\boldsymbol{A}}_{\boldsymbol{12}}\right)$ can also be observed and detected.

Therefore, the full state observer can be expressed as:

$$\hat{\bar{\boldsymbol{x}}}(t) = \begin{bmatrix}\hat{\bar{\boldsymbol{x}}}_{\boldsymbol{1}}\\ \hat{\bar{\boldsymbol{x}}}_{\boldsymbol{2}}\end{bmatrix} = \begin{bmatrix}\hat{\boldsymbol{y}}_{\boldsymbol{0}}(t)\\ \boldsymbol{w}(t) + \boldsymbol{L_r}\hat{\boldsymbol{y}}_{\boldsymbol{0}}(t)\end{bmatrix}, \tag{30}$$

where $\hat{\bar{\boldsymbol{x}}}_{\boldsymbol{1}}(t), \hat{\bar{\boldsymbol{x}}}_{\boldsymbol{2}}(t)$ are the observation of each state, $\boldsymbol{L_r} \in \mathbb{R}^{(n-n_0)\times n_0}$ is a constant gain matrix, utilized to guarantee the eigenvalue matrix $\bar{\boldsymbol{A}}_{\boldsymbol{22}} - \boldsymbol{L_r}\bar{\boldsymbol{A}}_{\boldsymbol{12}}$ stable. According to the observer design results, $\boldsymbol{w}(t) \in \mathbb{R}^{n-n_0}$ is expressed as follows:

$$\begin{aligned}\dot{\boldsymbol{w}}(t) &= \left(\bar{\boldsymbol{A}}_{\boldsymbol{22}} - \boldsymbol{L_r}\bar{\boldsymbol{A}}_{\boldsymbol{12}}\right)\boldsymbol{w}(t)\\ &+\left(\bar{\boldsymbol{B}}_{\boldsymbol{2}} - \boldsymbol{L_r}\bar{\boldsymbol{B}}_{\boldsymbol{1}}\right)\left(\boldsymbol{u_T}(t)+\boldsymbol{d}_{\boldsymbol{TM}}\right)\\ &+\left(\left(\bar{\boldsymbol{A}}_{\boldsymbol{22}} - \boldsymbol{L_r}\bar{\boldsymbol{A}}_{\boldsymbol{12}}\right)\boldsymbol{L_r} + \bar{\boldsymbol{A}}_{\boldsymbol{21}} - \boldsymbol{L_r}\bar{\boldsymbol{A}}_{\boldsymbol{11}}\right)\hat{\boldsymbol{y}}_{\boldsymbol{0}}(t)\end{aligned} \tag{31}$$

According to [22], if partial state observer is designed based on real state, i.e. $\hat{\boldsymbol{y}}_0(t) = \boldsymbol{y}_{\boldsymbol{0}}(t) = \boldsymbol{C_0}\boldsymbol{x}(t)$, then $\lim_{t\to\infty}\left(\boldsymbol{x}(t) - \hat{\boldsymbol{x}}(t)\right) = \lim_{t\to\infty}\boldsymbol{P}^{-1}\left(\bar{\boldsymbol{x}}(t) - \hat{\bar{\boldsymbol{x}}}(t)\right) = 0$, the state estimation error can achieve exponential convergence with the partial observer. Taking into account the observation error of the unified bounded state, the partial state observer will exponentially converge with bounded error, which is expressed as:

$$\lim_{t\to\infty}\sup\|\boldsymbol{x}(t) - \hat{\boldsymbol{x}}(t)\| = \lim_{t\to\infty}\sup\|\tilde{\boldsymbol{x}}(t)\| \le \rho_x.$$

where, $\tilde{\boldsymbol{x}}(t)$ is the full state observation error, and can be calculated as

$$\begin{aligned}\rho_x \le \left\|\boldsymbol{P}^{-1}\right\|\Big((1 + \|\boldsymbol{L_r}\| + \left\|\frac{\bar{\boldsymbol{B}}_{\boldsymbol{2}} - \boldsymbol{L_r}\bar{\boldsymbol{B}}_{\boldsymbol{1}}}{\bar{\boldsymbol{A}}_{\boldsymbol{22}} - \boldsymbol{L_r}\bar{\boldsymbol{A}}_{\boldsymbol{12}}}\right\|\rho_d\\ + \left\|\frac{\left(\bar{\boldsymbol{A}}_{22} - \boldsymbol{L_r}\bar{\boldsymbol{A}}_{12}\right)\boldsymbol{L_r} + \boldsymbol{A_{21}} - \boldsymbol{L_r}\bar{\boldsymbol{A}}_{\boldsymbol{11}}}{\bar{\boldsymbol{A}}_{\boldsymbol{22}} - \boldsymbol{L_r}\bar{\boldsymbol{A}}_{\boldsymbol{12}}}\right\|\Big)\rho_y)\end{aligned}$$

Computing (31-33) to solve $w(t)$ and denote

$$\begin{aligned}\boldsymbol{w}(t) &= \boldsymbol{\varepsilon_y}(t) + \boldsymbol{\varepsilon_0}(t) + \frac{\boldsymbol{N_2}(s)}{\Lambda(s)}[\boldsymbol{y_0}](t)\\ &+ \frac{\boldsymbol{N_1}(s)}{\Lambda(s)}\left(\boldsymbol{u_T}(t) + \boldsymbol{d}_{\boldsymbol{TM}}\right)\end{aligned} \tag{32}$$

where $\boldsymbol{\varepsilon_y}(t)$ is the observation error introduced by partial state, $\boldsymbol{\varepsilon_y}(t) = \left(s\boldsymbol{I} - \bar{\boldsymbol{A}}_{\boldsymbol{22}} + \boldsymbol{L_r}\bar{\boldsymbol{A}}_{\boldsymbol{12}}\right)^{-1} \times ((\bar{\boldsymbol{A}}_{\boldsymbol{22}} - \boldsymbol{L_r}\bar{\boldsymbol{A}}_{\boldsymbol{12}})\boldsymbol{L_r} + \bar{\boldsymbol{A}}_{\boldsymbol{21}} - \boldsymbol{L_r}\bar{\boldsymbol{A}}_{\boldsymbol{11}})[\tilde{\boldsymbol{y}}_{\boldsymbol{0}}](t)$, $\boldsymbol{\varepsilon_y}(t)$ is continuous and bounded. $\boldsymbol{\varepsilon_0}(t)$ represents the error caused by the initial value, $\boldsymbol{w}(0)$ is the estimation of $\boldsymbol{L_r}\boldsymbol{y_0}(0) - \bar{\boldsymbol{x}}_{\boldsymbol{2}}(0)$, $\Lambda(s) = \det\left(s\boldsymbol{I} - \bar{\boldsymbol{A}}_{\boldsymbol{22}} + \boldsymbol{L_r}\bar{\boldsymbol{A}}_{\boldsymbol{12}}\right)$, $\boldsymbol{N_1}(s)$, $\boldsymbol{N_2}(s)$ are $(n-n_0)\times M$ and $(n-n_0)\times n_0$ dimensional polynomial matrices. Thus, the observation partial state feedback controller can be expressed as:

$$\begin{aligned}\boldsymbol{K_1}^{*\mathrm{T}}\hat{\boldsymbol{x}}(t) &= \boldsymbol{\Theta_1}^{*\mathrm{T}}\frac{\boldsymbol{A_1}(s)}{\Lambda(s)}\left[\boldsymbol{u_T} + \hat{\boldsymbol{d}}_{\boldsymbol{TM}}\right](t)\\ &+ \boldsymbol{\Theta_{20}}^{*\mathrm{T}}\hat{\boldsymbol{y}}_{\boldsymbol{0}}(t) + \boldsymbol{\Theta_2}^{*\mathrm{T}}\frac{\boldsymbol{A_2}(s)}{\Lambda(s)}[\hat{\boldsymbol{y}}_{\boldsymbol{0}}](t) + \boldsymbol{K}^*_{\boldsymbol{p2}}\boldsymbol{\varepsilon_0}(t),\end{aligned} \tag{33}$$

where $\boldsymbol{K_1}^{*\mathrm{T}}\boldsymbol{P}^{-1} = \begin{bmatrix}\boldsymbol{K}^*_{\boldsymbol{p1}} & \boldsymbol{K}^*_{\boldsymbol{p2}}\end{bmatrix}$, $\boldsymbol{\Theta_{20}}^{*\mathrm{T}} = \boldsymbol{K}^*_{\boldsymbol{p1}} + \boldsymbol{K}^*_{\boldsymbol{p2}}\boldsymbol{L_r}$, $\boldsymbol{K}^*_{\boldsymbol{p2}}\boldsymbol{N_1}(s) = \boldsymbol{\Theta_1}^{*\mathrm{T}}\boldsymbol{A_1}(s)$, $\boldsymbol{K}^*_{\boldsymbol{p2}}\boldsymbol{N_2}(s) = \boldsymbol{\Theta_2}^{*\mathrm{T}}\boldsymbol{A_2}(s)$, $\boldsymbol{A_1}(s) = \left[\boldsymbol{I}_M, ..., s^{n-n_0-1}\boldsymbol{I}_M\right]^{\mathrm{T}}$, $\boldsymbol{A_2}(s) = \left[\boldsymbol{I_{n_0}}, ..., s^{n-n_0-1}\boldsymbol{I_{n_0}}\right]^{\mathrm{T}}$.

Based on the above derivation and $\boldsymbol{\Theta}^*_{\boldsymbol{3}} = \boldsymbol{K}^*_{\boldsymbol{2}}$, ignore the exponential decay term $\boldsymbol{K}^*_{\boldsymbol{p2}}\boldsymbol{\varepsilon_0}(t)$, the parameterized nominal partial state feedback controller with observation error can be obtained:

$$\begin{aligned}\boldsymbol{u_T}(t) &= \boldsymbol{\Theta_1}^{*\mathrm{T}}\hat{\boldsymbol{\omega}}_{\boldsymbol{1}}(t) + \boldsymbol{\Theta_2}^{*\mathrm{T}}\hat{\boldsymbol{\omega}}_{\boldsymbol{2}}(t)\\ &+ \boldsymbol{\Theta_{20}}^{*\mathrm{T}}\hat{\boldsymbol{y}}_{\boldsymbol{0}}(t) + \boldsymbol{\Theta}^*_{\boldsymbol{3}}\boldsymbol{r}(t) - \hat{\boldsymbol{d}}_{\boldsymbol{TM}}\end{aligned}, \tag{34}$$

where $\hat{\boldsymbol{\omega}}_{\boldsymbol{1}}(t) = \frac{\boldsymbol{A_1}(s)}{\Lambda(s)}\left(\boldsymbol{u_T}(t) + \hat{\boldsymbol{d}}_{\boldsymbol{TM}}\right)$,$\hat{\boldsymbol{\omega}}_{\boldsymbol{2}}(t) = \frac{\boldsymbol{A_2}(s)}{\Lambda(s)}[\hat{\boldsymbol{y}}_{\boldsymbol{0}}](t)$.

Remark 4.1: Compared with the partial state feedback control law based on real state given in [22], the estimation error introduced by the partial state observation information in this paper needs to be discussed. According to (33), with the estimation error mentioned above, the controller can be re-expressed as:

$$\begin{aligned}\boldsymbol{u_T}(t) &= \boldsymbol{\Theta_1}^{*\mathrm{T}}\frac{\boldsymbol{A_1}(s)}{\Lambda(s)}\left(\boldsymbol{u_T}(t) + \hat{\boldsymbol{d}}_{\boldsymbol{TM}}\right) + \boldsymbol{\Theta_2}^{*\mathrm{T}}\boldsymbol{\omega_2}(t)\\ &+ \boldsymbol{\Theta_{20}}^{*\mathrm{T}}\boldsymbol{y_0}(t) + \boldsymbol{\Theta}^*_{\boldsymbol{3}}r(t) - \hat{\boldsymbol{d}}_{\boldsymbol{TM}}\\ &+ \left(\boldsymbol{\Theta_2}^{*\mathrm{T}}\frac{\boldsymbol{A_2}(s)}{\Lambda(s)} + \boldsymbol{\Theta_{20}}^{*\mathrm{T}}\right)[\tilde{\boldsymbol{y}}_{\boldsymbol{0}}](t).\end{aligned} \tag{35}$$

The baseline controller will introduce the following additional input error:

$$\begin{aligned}\boldsymbol{\varepsilon_u}(t)=&\tilde{\boldsymbol{d}}_{\boldsymbol{TM}}+\frac{\left(\boldsymbol{\Theta_2}^{*\mathrm{T}}\frac{\boldsymbol{A_2}(s)}{\Lambda(s)}+\boldsymbol{\Theta_{20}}^{*\mathrm{T}}\right)[\tilde{\boldsymbol{y}}_{\mathbf{0}}](t)}{\boldsymbol{I_M}-\boldsymbol{\Theta_1}^{*\mathrm{T}}\frac{\boldsymbol{A_1}(s)}{\Lambda(s)}}+\boldsymbol{K_{p2}^*}\boldsymbol{\varepsilon_0}\\&=\tilde{\boldsymbol{d}}_{\boldsymbol{TM}}+\boldsymbol{K_1}^{*\mathrm{T}}\tilde{\boldsymbol{x}}(t).\end{aligned}\tag{36}$$

Considering the error introduced by the initial value of the observer $\boldsymbol{K_{p2}^*}\boldsymbol{\varepsilon_0}$ is exponential convergence, It can also be deduced that input error is continuously bounded, with the upper bound

$$\limsup_{t\to\infty}\|\boldsymbol{\varepsilon_u}(t)\|=\left\|\tilde{\boldsymbol{d}}_{\boldsymbol{TM}}\right\|+\left\|\boldsymbol{K_1}^{*\mathrm{T}}\right\|\|\tilde{\boldsymbol{x}}(t)\|\le\rho_d+\|\boldsymbol{K_1^*}\|\rho_x.$$

B. Model Output Matching Conditions

After discussing the observation error introduced by the control input, the controller is substituted into the closed-loop system, and discuss the output matching of the controller. [22] has discussed and proved the output matching of the object model based on the real partial state feedback controller, i.e. when $\boldsymbol{u_T}(t)=\boldsymbol{K_1}^{*\mathrm{T}}\hat{\boldsymbol{x}}(t)+\boldsymbol{K_2^*}\boldsymbol{r}(t)$, the nominal controller parameters $\boldsymbol{K_1^*}$ and $\boldsymbol{K_2^*}$ satisfy matching condition

$$\begin{aligned}&\boldsymbol{C}\left(s\boldsymbol{I}-\boldsymbol{A}-\boldsymbol{B}\boldsymbol{K_1}^{*\mathrm{T}}\right)^{-1}\boldsymbol{B}\boldsymbol{K_2^*}=\boldsymbol{W_m}(s),\\&\boldsymbol{K_2^{*-1}}=\boldsymbol{K_p}.\end{aligned}\tag{37}$$

The system can ensure the model output matching.

Aiming at the continuously bounded observation error of partial state, the output matching problem in this paper is expanded from [22], and continue to prove the output matching of the closed-loop system under the matching condition (39). Denote the following theorem:

Theorem 4.1: There exist constant parameters $\boldsymbol{\Theta_1^*},\boldsymbol{\Theta_2^*},\boldsymbol{\Theta_{20}^*},\boldsymbol{\Theta_3^*}$, such that the partial observation state based controller ensure the continuous boundedness of closed-loop signal and the model output matching tracking error $\boldsymbol{\varepsilon}(t)$ under any initial conditions.

Proof: The proof of the theorem will be divided into the following steps, including the convergence and boundedness of output matching tracking error, the existence of controller parameters and the boundedness of closed-loop systems.

The boundedness of the output matching tracking error. According to **Remark 4.1**, the controller input will introduce continuous bounded errors $\boldsymbol{\varepsilon_u}$ besides partial state estimation and observation disturbance errors. Note that the convergence process of the closed-loop system is firstly converge to the observation system through partial state feedback, then approach from the observation system to the real system, the convergence error of partial state observers and the input error will be considered comprehensively when matching the system output $\boldsymbol{y}(t)-\boldsymbol{y_m}(t)=\boldsymbol{\varepsilon}(t)$. Under the matching condition (37), the observer-based control law is expressed as:

$$\boldsymbol{u_T}=\boldsymbol{K_1}^{*\mathrm{T}}(\boldsymbol{x}(t)+\tilde{\boldsymbol{x}}(t))+\boldsymbol{K_2^*}\boldsymbol{r}(t)+\boldsymbol{d_{TM}}+\tilde{\boldsymbol{d}}_{\boldsymbol{TM}}.\tag{38}$$

Substituting (38) into (4) and obtain the system output:

$$\begin{aligned}\boldsymbol{y}(t)=&\boldsymbol{C}(s\boldsymbol{I}-\boldsymbol{A}-\boldsymbol{B}\boldsymbol{K_2^*})^{-1}\boldsymbol{B}\boldsymbol{K_2^*}[\boldsymbol{r}](t)\\&+\boldsymbol{C}\left(s\boldsymbol{I}-\boldsymbol{A}-\boldsymbol{B}\boldsymbol{K_1}^{*\mathrm{T}}\right)^{-1}\boldsymbol{B}(\boldsymbol{K_1}^{*\mathrm{T}}\tilde{\boldsymbol{x}}(t)+\tilde{\boldsymbol{d}}_{\boldsymbol{TM}}).\end{aligned}\tag{39}$$

The tracking error is expressed as:

$$\boldsymbol{\varepsilon}(t)=\boldsymbol{C}(s\boldsymbol{I}-\boldsymbol{A}-\boldsymbol{B}\boldsymbol{K_1}^{*\mathrm{T}})^{-1}\boldsymbol{B}(\boldsymbol{K_1}^{*\mathrm{T}}\tilde{\boldsymbol{x}}(t)+\tilde{\boldsymbol{d}}_{\boldsymbol{TM}})\tag{40}$$

It is seen that the system tracking error is continuously bounded as:

$$\begin{aligned}\lim_{t\to\infty}\sup\|\boldsymbol{\varepsilon}(t)\|&\le\left\|\boldsymbol{C}\left(s\boldsymbol{I}-\boldsymbol{A}-\boldsymbol{B}\boldsymbol{K_1}^{*\mathrm{T}}\right)^{-1}\boldsymbol{B}\right\|\|\boldsymbol{\varepsilon_u}(t)\|\\&\le\left\|\boldsymbol{C}\left(s\boldsymbol{I}-\boldsymbol{A}-\boldsymbol{B}\boldsymbol{K_1}^{*\mathrm{T}}\right)^{-1}\boldsymbol{B}\right\|(\rho_d+\|\boldsymbol{K_1^*}\|\rho_x)\end{aligned}$$

The existence of parameters. The controller parameters $\boldsymbol{\Theta_1^*},\boldsymbol{\Theta_2^*},\boldsymbol{\Theta_{20}^*},\boldsymbol{\Theta_3^*}$ influence model output matching the reference model output. The conclusion is derived from controller shown in the previous section.

The boundedness of closed-loop signals. From the previous derivation, it is known that closed-loop system output is bounded, i.e. $\boldsymbol{y}(t)=\boldsymbol{y_m}(t)+\boldsymbol{\varepsilon}(t)\in L^\infty$. Then the high-frequency gain matrix is utilized to inversely infer the boundedness of the system state. Note that

$$\begin{aligned}&\boldsymbol{\varepsilon}(t)=\boldsymbol{C}\left(s\boldsymbol{I}-\boldsymbol{A}-\boldsymbol{B}\boldsymbol{K_1}^{*\mathrm{T}}\right)^{-1}\boldsymbol{B}\boldsymbol{\varepsilon_u}(t)\\&=\boldsymbol{C}\left(s\boldsymbol{I}-\boldsymbol{A}-\boldsymbol{B}\boldsymbol{K_1}^{*\mathrm{T}}\right)^{-1}\boldsymbol{B}\\&\times\left(\tilde{\boldsymbol{d}}_{\boldsymbol{TM}}+\boldsymbol{K_{p2}^*}\boldsymbol{\varepsilon_0}(t)+\frac{\left(\boldsymbol{\Theta_2}^{*\mathrm{T}}\frac{\boldsymbol{A_2}(s)}{\Lambda(s)}+\boldsymbol{\Theta_{20}}^{*\mathrm{T}}\right)[\tilde{\boldsymbol{y}}_{\mathbf{0}}](t)}{\boldsymbol{I_M}-\boldsymbol{\Theta_1}^{*\mathrm{T}}\frac{\boldsymbol{A_1}(s)}{\Lambda(s)}}\right)\end{aligned}\tag{41}$$

then $\boldsymbol{\xi_m}(s)[\boldsymbol{\varepsilon}](t)$ can be expressed as the product of continuous bounded terms, $\boldsymbol{\xi_m}(s)[\boldsymbol{\varepsilon}](t)\in L^\infty$. As $\boldsymbol{\xi_m}(s)[\boldsymbol{y_m}](t)=\boldsymbol{r}(t)$, $\boldsymbol{\xi_m}(s)[\boldsymbol{y}](t)\in L^\infty$,

According to the essentially boundedness of the output signal, the boundedness of the closed-loop input signal $\boldsymbol{u}(t)$ is derived. By the full rank of $\boldsymbol{y}(t)=\boldsymbol{G}(s)(\boldsymbol{u_T}(t)+\boldsymbol{d_{TM}})$, and $\boldsymbol{G}(s)=\boldsymbol{C}(s\boldsymbol{I}-\boldsymbol{A})^{-1}\boldsymbol{B}$, ignoring the exponential decay effect of the initial conditions, it can be denoted

$$\boldsymbol{u_T}(t)=\boldsymbol{G}^{-1}(s)\boldsymbol{\xi_m^{-1}}(s)\boldsymbol{\xi_m}(s)[\boldsymbol{y}](t)-\boldsymbol{d_{TM}}.\tag{42}$$

Note that the external disturbance is also bounded, according to the stable assumption of $\boldsymbol{G}^{-1}(s)\boldsymbol{\xi_m^{-1}}(s)$, the controller input $\boldsymbol{u}(t)$ is bounded.

Finally, the boundedness of each state of the closed-loop system is discussed. For the observable system state parameter matrix $(\boldsymbol{A},\boldsymbol{C})$, the constant gain vector $\boldsymbol{L}\in\mathbb{R}^{n\times M}$, and the system state $\boldsymbol{x}(t)$ can be expressed as

$$\begin{aligned}\boldsymbol{x}(t)=&(s\boldsymbol{I}-\boldsymbol{A}+\boldsymbol{L}\boldsymbol{C})^{-1}\boldsymbol{B}(\boldsymbol{u_T}(t)+\boldsymbol{d_{TM}})\\&+(s\boldsymbol{I}-\boldsymbol{A}+\boldsymbol{L}\boldsymbol{C})^{-1}\boldsymbol{L}[\boldsymbol{y}](t)\\=&\frac{\boldsymbol{N_{01}}(s)}{\Lambda_0(s)}(\boldsymbol{u_T}(t)+\boldsymbol{d_{TM}})+\frac{\boldsymbol{N_{02}}(s)}{\Lambda_0(s)}[\boldsymbol{y}](t)\end{aligned}\tag{43}$$

where, the eigenvalue of matrix $\det A-\det LC$ is stable for $\boldsymbol{L}\in\mathbb{R}^{n\times M}$, $\Lambda_0(s)=det(s\boldsymbol{I}-\boldsymbol{A}+\boldsymbol{L}\boldsymbol{C})$, and configure $\boldsymbol{N_{01}}(s)=adj(s\boldsymbol{I}-\boldsymbol{A}+\boldsymbol{L}\boldsymbol{C})\boldsymbol{B}$ and $\boldsymbol{N_{02}}(s)=adj(s\boldsymbol{I}-\boldsymbol{A}+\boldsymbol{L}\boldsymbol{C})\boldsymbol{L}$ to the maximum dimension of $n-1$. Therefore, the internal state $\boldsymbol{x}(t)$ is

bounded and can be generalized to get the boundness of $\hat{\boldsymbol{y}}_{\boldsymbol{0}}(t)=\boldsymbol{C_0}\boldsymbol{x}(t)+\tilde{\boldsymbol{y}}_{\boldsymbol{0}}(t)$. ∇

Remark 4.2: the output matching of the parameter matrices $\boldsymbol{\Theta_1^*}\in\mathbb{R}^{M(n-n_0)\times M},\boldsymbol{\Theta_2^*}\in\mathbb{R}^{n_0(n-n_0)\times M},\boldsymbol{\Theta_{20}^*}\in\mathbb{R}^{n_0\times M},\boldsymbol{\Theta_3^*}\in\mathbb{R}^{M\times M}$ are given in [22] based on accurate state:

$$\begin{aligned}&\boldsymbol{\Theta_1}^{*\mathrm{T}}\boldsymbol{A_1}(s)\boldsymbol{P}(s)+(\boldsymbol{\Theta_2}^{*\mathrm{T}}\boldsymbol{A_2}(s)+\boldsymbol{\Theta_{20}}^{*\mathrm{T}}\Lambda(s))\boldsymbol{Z_0}(s)\\&=\Lambda(s)\left(\boldsymbol{P}(s)-\boldsymbol{\Theta_3}^{*\mathrm{T}}\boldsymbol{k_p}\boldsymbol{\xi_m}(s)\boldsymbol{Z}(s)\right),\end{aligned}\tag{44}$$

where, $\boldsymbol{G}(s)=\boldsymbol{Z}(s)\boldsymbol{P}^{-1}(s),\boldsymbol{G_0}(s)=\boldsymbol{Z_0}(s)\boldsymbol{P}^{-1}(s)$, and $\boldsymbol{y_0}(t)=\boldsymbol{G_0}(s)[\boldsymbol{u_T}](t),\boldsymbol{G_0}(s)=\boldsymbol{C_0}(s\boldsymbol{I}-\boldsymbol{A})^{-1}\boldsymbol{B}$. When the disturbance estimation feedback and partial observation state are considered in the controller design, the input-output relationship of the state is updated as:

$$\hat{\boldsymbol{y}}_{\boldsymbol{0}}(t)=\boldsymbol{G_0}(s)(\boldsymbol{u_T}(t)+\boldsymbol{d_{TM}})+\tilde{\boldsymbol{y}}_{\boldsymbol{0}}.\tag{45}$$

Taking into account that $\tilde{\boldsymbol{y}}_{\boldsymbol{0}}$ is bounded, the output matching condition is relaxed and the closed-loop system output tracking is allowed to have continuous bounded errors. The matching relationship of closed-loop transfer function is given according to the baseline requirements:

$$\begin{aligned}&\boldsymbol{I_M}-\boldsymbol{\Theta_1}^{*\mathrm{T}}\frac{\boldsymbol{A_1}(s)}{\Lambda(s)}-\left(\boldsymbol{\Theta_2}^{*\mathrm{T}}\frac{\boldsymbol{A_2}(s)}{\Lambda(s)}+\boldsymbol{\Theta_{20}}^{*\mathrm{T}}\right)\boldsymbol{G_0}(s)\\&=\boldsymbol{\Theta_3^*}\boldsymbol{W_m^{-1}}(s)\boldsymbol{G}(s)\end{aligned}\tag{46}$$

It shows that the nominal parameter matrix output matching is still applicable to the observation state feedback control scheme in this paper, but the upper bound of the tracking error will be introduced as $\left\|\boldsymbol{C}\left(s\boldsymbol{I}-\boldsymbol{A}-\boldsymbol{B}\boldsymbol{K_1^{*T}}\right)^{-1}\boldsymbol{B}\right\|(\rho_d+\|\boldsymbol{K_1^*}\|\rho_x)$.

C. Adaptive Controller Design

The adaptive control scheme aims to solve the problem of nonlinear uncertainties in the system state parameter matrix $(\boldsymbol{A},\boldsymbol{B},\boldsymbol{C})$. Considering that the adaptive estimation of the three state matrices in the time domain model will further increase the difficulty of designing the adaptive update law, according to [24], the high-frequency gain decomposition is introduced to simplify the adaptive approximation process and reduce the difficulty of controller design. Given the following assumptions:

Assumption 4.2: All sequential principal minor $\boldsymbol{\Delta_i},i=1,2,...,M$ of the high-frequency matrix $\boldsymbol{K_p}$ are non-zero with the symbols known. Such $\boldsymbol{K_p}$ has a non-unique high-frequency gain decomposition:

$$\boldsymbol{K_p}=\boldsymbol{L_s}\boldsymbol{D_s}\boldsymbol{S},\tag{47}$$

where $\boldsymbol{S}=\boldsymbol{S}^{\mathrm{T}}>0,\boldsymbol{L_s}\in\mathbb{R}^{M\times M}$ is a unit upper triangle matrix, $\boldsymbol{D_s}=diag[s_1^*,s_2^*,...,s_M^*]=diag[sign[d_1^*]\gamma_1,...,sign[d_M^*]\gamma_M]$ has arbitrary and selected constants $\gamma_i>0,i=1,2,...,M$.

Adaptive partial observation state feedback control framework: Similar to the nominal state feedback control, the adaptive version of the partial observation state feedback control is expressed as:

$$\begin{aligned}\boldsymbol{u_T}(t)=&\hat{\boldsymbol{\Theta}}_{\boldsymbol{1}}{}^{\mathrm{T}}(t)\frac{\boldsymbol{A_1}(s)}{\Lambda(s)}\left(\boldsymbol{u}(t)+\hat{\boldsymbol{d}}_{\boldsymbol{TM}}\right)+\hat{\boldsymbol{\Theta}}_{\boldsymbol{3}}(t)\boldsymbol{r}(t)\\&+\left(\hat{\boldsymbol{\Theta}}_{\boldsymbol{2}}{}^{\mathrm{T}}(t)\frac{\boldsymbol{A_2}(s)}{\Lambda(s)}+\hat{\boldsymbol{\Theta}}_{\boldsymbol{20}}{}^{\mathrm{T}}(t)\right)\hat{\boldsymbol{y}}_{\boldsymbol{0}}(t)-\hat{\boldsymbol{d}}_{\boldsymbol{TM}},\end{aligned}\tag{48}$$

where $\hat{\boldsymbol{\Theta}}_{\boldsymbol{1}},\hat{\boldsymbol{\Theta}}_{\boldsymbol{2}},\hat{\boldsymbol{\Theta}}_{\boldsymbol{20}},\hat{\boldsymbol{\Theta}}_{\boldsymbol{3}}$ are the adaptive estimations of $\boldsymbol{\Theta_1^*},\boldsymbol{\Theta_2^*},\boldsymbol{\Theta_{20}^*},\boldsymbol{\Theta_3^*}$ respectively.

Tracking error equation: The tracking error has been discussed during the derivation of the nominal partial state feedback, which shows that the nominal tracking error is also continuously bounded when the bounded observation error of the partial state and additional disturbance exists. Similarly, according to the system output matching equation, it can be obtained:

$$\begin{aligned}&\left(\boldsymbol{I_M}-\boldsymbol{\Theta_1}^{*\mathrm{T}}\frac{\boldsymbol{A_1}(s)}{\Lambda(s)}\right)(\boldsymbol{u_T}(t)+\boldsymbol{d_{TM}})\\&-\left(\boldsymbol{\Theta_2}^{*\mathrm{T}}\frac{\boldsymbol{A_2}(s)}{\Lambda(s)}+\boldsymbol{\Theta_{20}}^{*\mathrm{T}}\right)\boldsymbol{y_0}(t)-\boldsymbol{\Theta_3^*}\boldsymbol{W_m^{-1}}(s)[\boldsymbol{y}](t)\\&=\boldsymbol{C}\left(s\boldsymbol{I}-\boldsymbol{A}-\boldsymbol{B}\boldsymbol{K_1}^{*\mathrm{T}}\right)^{-1}\boldsymbol{B}\\&\times\left(\tilde{\boldsymbol{d}}_{\boldsymbol{TM}}+\boldsymbol{K_{p2}^*}\boldsymbol{\varepsilon_0}(t)+\frac{\left(\boldsymbol{\Theta_2}^{*\mathrm{T}}\frac{\boldsymbol{A_2}(s)}{\Lambda(s)}+\boldsymbol{\Theta_{20}}^{*\mathrm{T}}\right)[\tilde{\boldsymbol{y}}_{\boldsymbol{0}}](t)}{\boldsymbol{I_M}-\boldsymbol{\Theta_1}^{*\mathrm{T}}\frac{\boldsymbol{A_1}(s)}{\Lambda(s)}}\right)\end{aligned}\tag{49}$$

Organize the above equations,the tracking error can be expressed as:

$$\begin{aligned}\boldsymbol{e}(t)&=\boldsymbol{y}(t)-\boldsymbol{y_m}(t)\\&=\boldsymbol{W_m}(s)\boldsymbol{K_p}\left[\boldsymbol{u_T}-\boldsymbol{\Theta}^{*\mathrm{T}}\hat{\boldsymbol{\omega}}+\boldsymbol{\varepsilon_u}\right](t),\end{aligned}\tag{50}$$

where, $\hat{\boldsymbol{\omega}}(t)=\left[\hat{\boldsymbol{\omega}}_{\boldsymbol{1}}{}^{\mathrm{T}}(t),\hat{\boldsymbol{\omega}}_{\boldsymbol{2}}{}^{\mathrm{T}}(t),\hat{\boldsymbol{y}}_{\boldsymbol{0}}{}^{\mathrm{T}}(t),\boldsymbol{r}^{\mathrm{T}}(t)\right]^{\mathrm{T}}$, correspondingly, $\boldsymbol{\Theta}^*=\left[\boldsymbol{\Theta_1}^{*\mathrm{T}},\boldsymbol{\Theta_2^{*T}},\boldsymbol{\Theta_{20}}^{*\mathrm{T}},\boldsymbol{\Theta_3^*}\right]^{\mathrm{T}}$. It can conclude that the adaptive control scheme implemented by the error tracking equation is actually utilized to achieve the approximation process of the system input to the nominal input.

Estimation error equation based on the high-frequency gain decomposition. After expressing the system tracking error as a function of the high-frequency gain matrix $\boldsymbol{K_p}$, the decomposition of $\boldsymbol{K_p}$ can be used to express the adaptive variables parametrically. Substituting the hdecomposition of $\boldsymbol{K_p}$ in (47) into the tracking error equation, utilizing the adaptive controller given in (48) to rewrite (50) as:

$$\boldsymbol{e}(t)=\boldsymbol{\xi_m^{-1}}(s)\boldsymbol{L_s}\boldsymbol{D_s}\boldsymbol{S}\left(\left(\hat{\boldsymbol{\Theta}}^{\mathrm{T}}-\boldsymbol{\Theta}^{*\mathrm{T}}\right)\hat{\boldsymbol{\omega}}(t)+\boldsymbol{\varepsilon_u}(t)\right),\tag{51}$$

where, $\hat{\boldsymbol{\Theta}}^{\mathrm{T}}=\left[\hat{\boldsymbol{\Theta}}_{\boldsymbol{1}},\hat{\boldsymbol{\Theta}}_{\boldsymbol{2}},\hat{\boldsymbol{\Theta}}_{\boldsymbol{20}},\hat{\boldsymbol{\Theta}}_{\boldsymbol{3}}\right]^{\mathrm{T}}$. In order to parameterize the unknown upper triangular matrix $\boldsymbol{L_s}$, a constant matrix $\boldsymbol{\Theta_0^*}=\boldsymbol{L_s^{-1}}-\boldsymbol{I}=\left\{\theta_{ij}^*\right\}$ is introduced, where $\theta_{ij}^*=0,i=1,2,...,M,j\geq i$, and define the parameter matrix estimation error as $\tilde{\boldsymbol{\Theta}}(t)=\boldsymbol{\Theta}(t)-\boldsymbol{\Theta}^*(t)$, further rewrite (51) as:

$$\boldsymbol{\xi_m}(s)[e](t)+\boldsymbol{\Theta_0^*}\boldsymbol{\xi_m}(s)[\boldsymbol{e}](t)=\boldsymbol{D_s}\boldsymbol{S}\left[\tilde{\boldsymbol{\Theta}}^{\mathrm{T}}\hat{\boldsymbol{\omega}}+\boldsymbol{\varepsilon_u}\right](t).\tag{52}$$

Further parameterize (52) and introduce a stable single polynomial $f(s)$ which dimension is equal to the maximum dimension of $\boldsymbol{\xi_m}(s)$. Utilizing the filter $h(s) = 1/f(s)$ to correct the tracking error, and formulate as:

$$\begin{aligned}&\boldsymbol{\xi_m}(s)\, h(s)\, [\boldsymbol{e}](t) + \boldsymbol{\Theta_0^*}\boldsymbol{\xi_m}(s)\, h(s)\, [\boldsymbol{e}](t)\\ &= \boldsymbol{D_s S} h(s) \left[\tilde{\boldsymbol{\Theta}}^{\mathbf{T}}\hat{\boldsymbol{\omega}} + \boldsymbol{\varepsilon_u}\right](t).\end{aligned} \tag{53}$$

Let

$$\begin{aligned}&\bar{\boldsymbol{e}}(t) = \boldsymbol{\xi_m}(s)\, h(s)\, [\boldsymbol{e}](t) = [\bar{\boldsymbol{e}}_{\mathbf{1}}(t), ..., \bar{\boldsymbol{e}}_{\boldsymbol{M}}(t)]^{\mathrm{T}}\\ &\boldsymbol{\eta_i}(t) = [\bar{\boldsymbol{e}}_{\mathbf{1}}(t), ..., \bar{\boldsymbol{e}}_{\boldsymbol{i-1}}(t)]^{\mathrm{T}} \in \mathbb{R}^{i-1},\\ &\boldsymbol{\theta_i^*} = \left[\boldsymbol{\theta_{i1}^*}, ..., \boldsymbol{\theta_{ii-1}^*}\right]^{\mathrm{T}}, i = 2, ..., M,\end{aligned} \tag{54}$$

then (53) is expressed as

$$\begin{aligned}&\bar{\boldsymbol{e}}(t) + \left[\mathbf{0}, \boldsymbol{\theta_2}^{*\mathrm{T}}\boldsymbol{\eta}_2(t), \boldsymbol{\theta_3}^{*\mathrm{T}}\boldsymbol{\eta}_3(t), ..., \boldsymbol{\theta_M}^{*\mathrm{T}}\boldsymbol{\eta}_M(t)\right]^{\mathrm{T}}\\ &= \boldsymbol{D_s S} h(s) \left[\tilde{\boldsymbol{\Theta}}^{\mathrm{T}}\hat{\boldsymbol{\omega}} + \boldsymbol{\varepsilon_u}\right](t).\end{aligned} \tag{55}$$

To achieve the object tracking, the model output needs to be realized, i.e. the convergence of the high-frequency gain matrix and the controller parameters to the nominal value is required. Define the overall estimation error $\boldsymbol{\upsilon}(t)$ containing the parameter estimation error, expressed as:

$$\begin{aligned}\boldsymbol{\upsilon}(t) &= \left[\mathbf{0}, \hat{\boldsymbol{\theta}}_{\mathbf{2}}^{\mathrm{T}}\boldsymbol{\eta_2}(t), ..., \hat{\boldsymbol{\theta}}_{\boldsymbol{M}}^{\mathrm{T}}\boldsymbol{\eta_M}(t)\right]^{\mathrm{T}} + \bar{\boldsymbol{e}}(t)\\ &+ \hat{\boldsymbol{\Psi}}(t)\left(\hat{\boldsymbol{\Theta}}^{\mathbf{T}}(t)\, h(s)\, [\hat{\boldsymbol{\omega}}](t) - h(s)\left[\hat{\boldsymbol{\Theta}}^{\mathrm{T}}\hat{\boldsymbol{\omega}}\right](t)\right),\end{aligned} \tag{56}$$

where, $\hat{\boldsymbol{\theta}}_{\boldsymbol{i}}(t), i = 2, ..., M, \hat{\boldsymbol{\Psi}}(t)$ are the adaptive parameter matrix estimations of $\boldsymbol{L_s}$ and $\boldsymbol{D_s S}$. Simplify (56) to obtain the linear form of parameter estimation and tracking error to update the adaptive law, derived the estimation error and expressed as follows:

$$\begin{aligned}\boldsymbol{\upsilon}(t) &= \left[\mathbf{0}, \hat{\boldsymbol{\theta}}_{\mathbf{2}}^{\mathrm{T}}\boldsymbol{\eta_2}(t), ..., \hat{\boldsymbol{\theta}}_{\boldsymbol{M}}^{\mathrm{T}}\boldsymbol{\eta_M}(t)\right]^{\mathrm{T}} + \bar{\boldsymbol{e}}(t)\\ &+ \hat{\boldsymbol{\Psi}}(t)\left(\hat{\boldsymbol{\Theta}}^{\mathrm{T}}(t)\, h(s)\, [\hat{\boldsymbol{\omega}}](t) - h(s)\left[\hat{\boldsymbol{\Theta}}^{\mathrm{T}}\hat{\boldsymbol{\omega}}\right](t)\right)\\ &= \left[\mathbf{0}, \tilde{\boldsymbol{\theta}}_{\mathbf{2}}^{\mathrm{T}}\boldsymbol{\eta_2}(t), ..., \tilde{\boldsymbol{\theta}}_{\boldsymbol{M}}^{\mathrm{T}}\boldsymbol{\eta_M}(t)\right]^{\mathrm{T}}\\ &+ \tilde{\boldsymbol{\Psi}}(t)\left(\hat{\boldsymbol{\Theta}}^{\mathrm{T}}(t)\, h(s)\, [\hat{\boldsymbol{\omega}}](t) - h(s)\left[\hat{\boldsymbol{\Theta}}^{\mathrm{T}}\hat{\boldsymbol{\omega}}\right](t)\right)\\ &+ \boldsymbol{D_s S}\tilde{\boldsymbol{\Theta}}^{\mathrm{T}}(t)\, h(s)\, [\hat{\boldsymbol{\omega}}](t) + \boldsymbol{D_s S} h(s)\, [\boldsymbol{\varepsilon_u}](t),\end{aligned} \tag{57}$$

where $\tilde{\boldsymbol{\theta}}_{\boldsymbol{i}}(t) = \hat{\boldsymbol{\theta}}(t) - \boldsymbol{\theta_i^*}, i = 2, ..., M, \tilde{\boldsymbol{\Psi}}(t) = \hat{\boldsymbol{\Psi}}(t) - \boldsymbol{\Psi}^*$ is the parameter estimation error of the high-frequency gain matrix, $\boldsymbol{\Psi}^* = \boldsymbol{D_s S}$.

Adaptive update law. When designing an adaptive law based on the observation state, the tracking error is unknown caused by uncertainties, which only yields

$$\hat{\boldsymbol{e}}(t) = \hat{\boldsymbol{y}}(t) - \boldsymbol{y_m}(t) = \boldsymbol{W_m}(s)\, \boldsymbol{K_p}\left[\boldsymbol{u_T} - \boldsymbol{\Theta}^{*\mathrm{T}}\hat{\boldsymbol{\omega}}\right](t). \tag{58}$$

The adaptive laws are obtained as

$$\begin{aligned}&\dot{\hat{\boldsymbol{\theta}}}_{\boldsymbol{i}}(t) = -\frac{\boldsymbol{\Gamma_{\theta_i}}\boldsymbol{\upsilon}(t)\, \boldsymbol{\eta_i}(t)}{m^2(t)}, i = 2, 3, ..., M,\\ &\dot{\hat{\boldsymbol{\Theta}}}^{\mathrm{T}}(t) = -\frac{\boldsymbol{D_s}\boldsymbol{\upsilon}(t)\, [h(s)\, [\hat{\boldsymbol{\omega}}]]^{\mathrm{T}}(t)}{m^2(t)},\\ &\dot{\hat{\boldsymbol{\Psi}}}(t) = -\frac{\boldsymbol{\Gamma_\Psi}\boldsymbol{\upsilon}(t)\left[\left[\hat{\boldsymbol{\Theta}}^{\mathrm{T}}\right] h(s)\, [\hat{\boldsymbol{\omega}}] - h(s)\left[\hat{\boldsymbol{\Theta}}^{\mathrm{T}}\hat{\boldsymbol{\omega}}\right]\right]^{\mathrm{T}}(t)}{m^2(t)},\end{aligned} \tag{59}$$

where, $\boldsymbol{\Gamma_{\theta_i}}, \boldsymbol{\Gamma_\Psi}$ are the adaptive gain matrices, which satisfy $\boldsymbol{\Gamma} = \boldsymbol{\Gamma}^{\mathrm{T}} > 0$, parameter m is given as:

$$\begin{aligned}&m^2(t) = 1 + [h(s)\, [\hat{\boldsymbol{\omega}}]]^{\mathrm{T}}(t)\, [h(s)\, [\hat{\boldsymbol{\omega}}]](t)\\ &+ \sum_{i=2}^{M} \boldsymbol{\eta_i}^{\mathrm{T}}(t)\boldsymbol{\eta_1}(t) + \left[\left[\hat{\boldsymbol{\Theta}}^{\mathrm{T}}\right] h(s)\, [\hat{\boldsymbol{\omega}}] - h(s)\left[\hat{\boldsymbol{\Theta}}^{\mathrm{T}}\hat{\boldsymbol{\omega}}\right]\right]^{\mathrm{T}}(t)\\ &\times \left[\left[\hat{\boldsymbol{\Theta}}^{\mathrm{T}}\right] h(s)\, [\hat{\boldsymbol{\omega}}] - h(s)\left[\hat{\boldsymbol{\Theta}}^{\mathrm{T}}\hat{\boldsymbol{\omega}}\right]\right](t).\end{aligned}$$

To analyse the stability of the close loop signals and the convergence of output tracking error, the theorem is shown as follows:

Theorem 4.2: Subject the feedback controller (48), reconfigurable fault-tolerant controller (28), adaptive laws (61), and control plant (4) to the drag-free closed-loop system, ensuring each signal bounded and output tracking error $\boldsymbol{e}(t) = \boldsymbol{y}(t) - \boldsymbol{y_m}(t)$ convergence, the L^2 norm upper bound of the vector is not greater than $\|\boldsymbol{W_m}(s)\, \boldsymbol{K_3}(s)\, \boldsymbol{D_s S}(\rho_d + \rho_r + \|\boldsymbol{K_1^*}\|\rho_x)\|$ with actuator faults shown in (8).

The proof of **Theorem 4.2** can be obtained in a similar way as [22]. To derive the stability accurancy of the output signals, a detailed proof is obtained in **Appendix**.

V. SIMULATION RESULTS AND ANALYSIS

A. Parameter Settings

In the simulation, the step length is set to be 0.1 s, and the control performance of the baseline partial observation state feedback MRAC and the FTC system are verified respectively. The simulation time is set to be 500 s. The noise $\boldsymbol{d_{TM}}$ refers to [17]. According to [17], for the dynamic modeling of the drag-free control system, the stiffness matrix is set as

$$\boldsymbol{\Omega_{DF}^2} = 10^{-7} \times (1 \pm 5\%) \times \begin{bmatrix} 11.19 & 1.35 & 1.35 & 0.00425 & 0 & 0\\ 1.35 & 9.55 & 1.35 & 0.00425 & 0 & 0\\ 1.35 & 1.35 & 24.12 & 0.00425 & 0 & 0\\ 26.087 & 26.087 & 26.087 & 30.64 & 0 & 0\\ 0 & 0 & 0 & 0 & 9.55 & 1.35\\ 0 & 0 & 0 & 0 & 1.35 & 24.12 \end{bmatrix},$$

and the input matrix is set as

$$\boldsymbol{B_{DF}} = \begin{bmatrix} -1 & 0 & 0 & 0 & 0 & 0\\ 0 & -1 & 0 & 0.45 & 0 & 0\\ 0 & 0 & -1 & 0 & 0 & 0\\ 0 & 0 & 0 & -1 & 0 & 0\\ 0 & 0 & 0 & 0 & -1 & 0\\ 0 & 0 & 0 & 0 & 0 & -1 \end{bmatrix}.$$

In the numerical simulation of the baseline controller, the H_∞ control scheme and the QFT quantitative feedback control scheme are introduced to compare with the scheme designed in this paper. The z_1, z_2 axes state $[\dot{z}_1, z_1, \dot{z}_2, z_2]^{\mathrm{T}}$ is observed by the remaining 4-DOF state.

The observer gain $\boldsymbol{L}$ is set as

$$\boldsymbol{L}=\begin{bmatrix}1 & 1 & 0 & 0 & 0 & 0 & 0 & 0\\ 1 & 1 & 0.02 & 0.22 & 0 & 0 & 0 & 0\\ 1 & 1 & 0 & 0 & 0 & 0.11 & 0 & 0\\ 0 & 1 & 0 & 1 & 0.07 & 0.11 & 0.07 & 0.11\end{bmatrix}.$$

The left interaction matrix is modified as $\boldsymbol{\xi_m}(s) = \left(s+8\times10^{-7}\right)\cdot I_{8\times8}$, the adaptive gains are set to be $\Gamma_\theta = 0.001\cdot\boldsymbol{I}_{5\times5}$, $\Gamma_\Psi = 1\cdot\boldsymbol{I}_{8\times8}$.

In the simulation verification of the reconfigurable fault-tolerant controller, the bias fault $\bar{u}_i$ introduced by each actuator are constant values, $\bar{u}_1 = -5\times10^{-12}, \bar{u}_2 = -4\times10^{-11}, \bar{u}_3 = -1.2\times10^{-11}$, $\bar{u}_4 = -7\times10^{-12}, \bar{u}_5 = \bar{u}_6 = -2\times10^{-11}$. The initial value of $\hat{u}_{T_{\delta_0}}$ in the six sensitive axes when the fault detection triggers is set to be $\hat{u}_{T_{\delta_0}} = [-7.2,-7,-8.4,-12.2,-7,-8.4]^{\mathrm{T}}\times10^{-12}$. Before the fault is detected, the initial value of $\hat{u}_{T_{\delta_0}}$ is 0. The fault observer gains of the comparison scheme in [25] and the proposed scheme in this work are set to be the same, $\boldsymbol{k_1} = 0.1\cdot\boldsymbol{I}_{6\times6}$ and $\boldsymbol{l_1} = 1.6\cdot\boldsymbol{I}_{6\times6}$. The constructed sequence has 20 iterations in each channel.

B. Simulation Verification and Analysis

To support our theoretical analysis, the simulation results are divided into two parts. The control performance of the proposed MRAC scheme is verified by comparing to the H_∞ [2] scheme and QFT [3] scheme in the first part, while the efficiency of the fault observer is verified by comparing the typical fault observer [25] in the second part. Numerical simulation is performed based on the sample space gravitational wave detection satellite in [17], and the control performance of the nominal partial observation state feedback MRAC scheme and the reconfigurable fault-tolerant controller are verified in the time domain and frequency domain. The simulation results are shown in Fig. 3 to Fig. 13 and are analyzed as follows:

Verification of baseline partial observation state feedback MRAC control scheme: Introducing QFT quantitative feedback control scheme [3] and H_∞ robust control scheme [2], compared with the MRAC scheme in x_1, y_1, θ_1, y_2 axes. The simulation results are shown in Fig. 3-6. Which show that in the sensitive axis x_1, the MRAC scheme improves the disturbance suppression ability by 70% compared with the linear robust control schemes, and the disturbance suppression ability on the other non-sensitive axes increases by $30\% - 80\%$. As a nonlinear control scheme, the MRAC scheme has better nonlinear approximation ability than the other two linear control methods, and has a better adaptive disturbance suppression effect in response to system observation errors and other uncertainties. In view of the requirement satisfaction of the sensitive axis residual acceleration. Fig. 7 shows the residual acceleration frequency domain simulation result, which verifies that the MRAC scheme meets the requirement of detection, and also verifies the performance improvement effect of its comparison with other convention schemes. The frequency domain simulation also reflects the z_1, z_2 axes displacement and acceleration performance. As shown in Fig. 8-11, the MRAC scheme meets the performance requirements of the sample detection mission.

TABLE I

Parameter Sets of Observer (15).

Order of sets	observer gain $\boldsymbol{k_1}$	observer gain $\boldsymbol{l_1}$
1	$\boldsymbol{k_1} = 0.05\cdot\boldsymbol{I}_{6\times6},$	$\boldsymbol{l_1} = 0.8\cdot\boldsymbol{I}_{6\times6},$
2	$\boldsymbol{k_1} = 0.1\cdot\boldsymbol{I}_{6\times6},$	$\boldsymbol{l_1} = 0.8\cdot\boldsymbol{I}_{6\times6},$
3	$\boldsymbol{k_1} = 0.15\cdot\boldsymbol{I}_{6\times6},$	$\boldsymbol{l_1} = 1.0\cdot\boldsymbol{I}_{6\times6},$
4	$\boldsymbol{k_1} = 0.2\cdot\boldsymbol{I}_{6\times6},$	$\boldsymbol{l_1} = 1.0\cdot\boldsymbol{I}_{6\times6},$
5	$\boldsymbol{k_1} = 0.1\cdot\boldsymbol{I}_{6\times6},$	$\boldsymbol{l_1} = 1.6\cdot\boldsymbol{I}_{6\times6},$

Fault tolerant ability verification of reconfigurable control scheme based on sequential Lyapunov method: Introduce constant bias faults into the first-order actuator loops of the baseline control system $\bar{u}_i, i = 1,2,...,6$, utilizing sequential Lyapunov method to iteratively reconfigurable input and verify the fault tolerant ability in 6-DOF drag-free loops. The simulation results are shown in Fig. 12 to Fig.15. The motivation of our proposed sequence Lyapunov scheme based method is to decrease the estimation error of the commonly used observer (15) by the iterative procedure in **Algorithm 3.1**. According to Fig. 12 and Fig. 13, we compare the performance between the observer (15) and the proposed sequence Lyapunov scheme based observer. Fig.13 depicts the actual fault and fault estimation results derived from observer (15) under 5 different sets of parameters in x, y and z axes given in TABLE I, with the fault estimation denoted as:

$$\begin{aligned}\hat{\tilde{\boldsymbol{u}}}_0 =& -\left(\boldsymbol{l_1}-\boldsymbol{I}\right)\left(\boldsymbol{l_1}\boldsymbol{k_1}+\boldsymbol{I}\right)^{-1}\boldsymbol{l_1}\boldsymbol{k_1}\boldsymbol{S}\\ &+\left(\left(\boldsymbol{l_1}-\boldsymbol{I}\right)\left(\boldsymbol{l_1}\boldsymbol{k_1}+\boldsymbol{I}\right)^{-1}\boldsymbol{l_1}\boldsymbol{k_1}-\boldsymbol{l_1}\right)\tilde{\boldsymbol{u}}_{T_\delta},\end{aligned}$$

from which we observe that there is a large deviation between the actual fault and the estimated ones. Therefore, the commonly used observer (15) need to be enhanced to improve the estimation accuracy. On the other hand, as shown in Fig. 13, the proposed observe achieves better estimation accuracy than that of observer (15). Moreover, since the fault estimation accuracy is improved by the proposed observer, the FTC scheme can exhibit good fault-tolerant capability in each drag-free channel, as illustrated in Fig. 14 and Fig. 15.

VI. CONCLUSION

Aiming at the precision and stability problem of the drag-free control system of space detection spacecraft, an MRAC scheme is proposed in this paper based on partial observation state feedback. To realize the actuator bias fault tolerant performance, a retrofit control method based on the sequence Lyapunov method is designed to achieve FTC scheme. Specifically, the sequential Lyapunov method is utilized to realize the simultaneous detection of the two types of state information in the

This article has been accepted for publication in IEEE Transactions on Aerospace and Electronic Systems. This is the author's version which has not been fully edited and content may change prior to final publication. Citation information: DOI 10.1109/TAES.2023.3276342

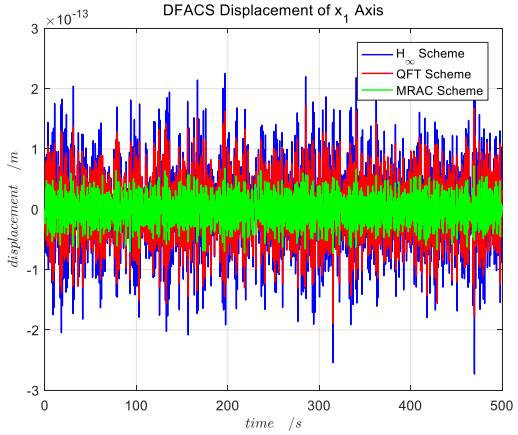

Fig. 3. Displacement noise comparison between the baseline MRAC scheme and other schemes in x_1 axis.

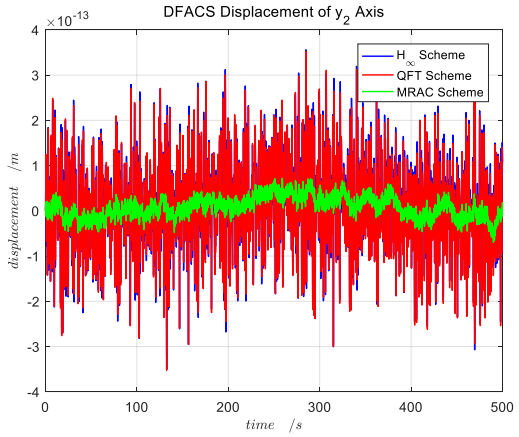

Fig. 6. Displacement noise comparison between the baseline MRAC scheme and other schemes in y_2 axis.

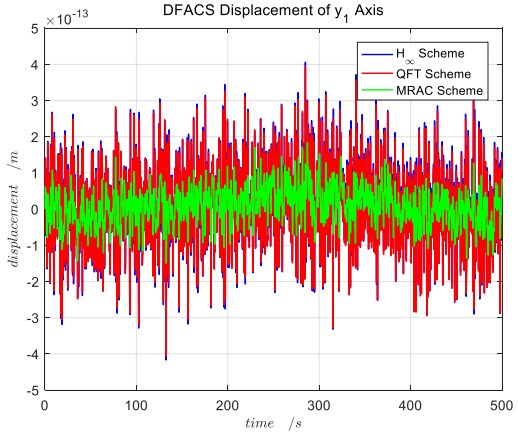

Fig. 4. Displacement noise comparison between the baseline MRAC scheme and other schemes in y_1 axis.

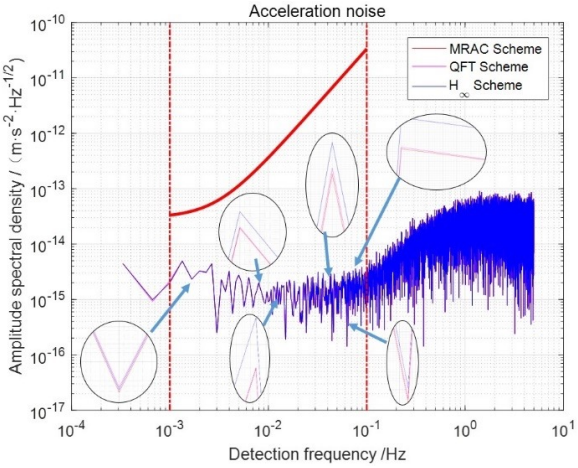

Fig. 7. Comparison of residual acceleration between the MRAC scheme and other schemes in the sensitive axis.

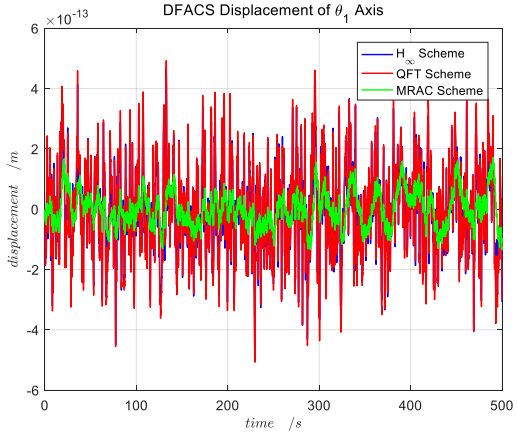

Fig. 5. Displacement noise comparison between the baseline MRAC scheme and other schemes in θ_1 axis.

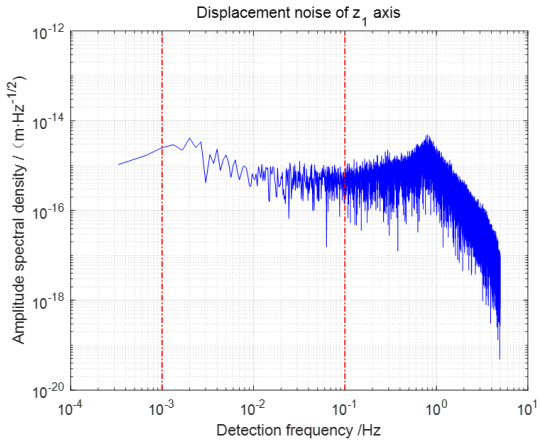

Fig. 8. Displacement noise of the MRAC scheme in z_1 axis.

This article has been accepted for publication in IEEE Transactions on Aerospace and Electronic Systems. This is the author's version which has not been fully edited and content may change prior to final publication. Citation information: DOI 10.1109/TAES.2023.3276342

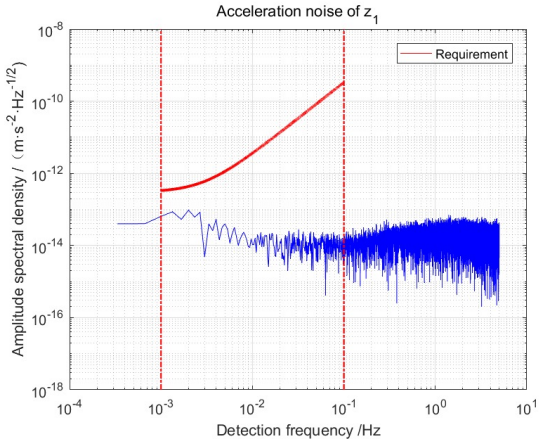

Fig. 9. Acceleration noise of the MRAC scheme in z_1 axis.

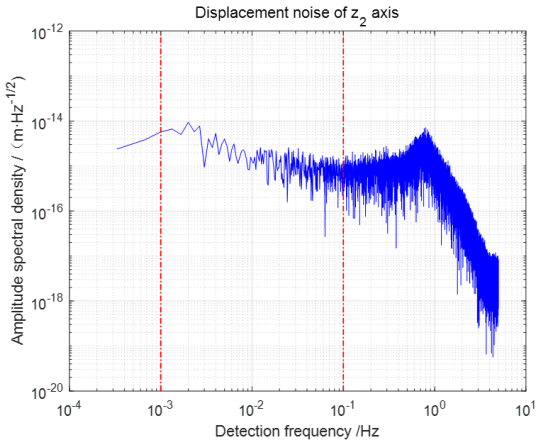

Fig. 10. Displacement noise of the MRAC scheme in z_2 axis.

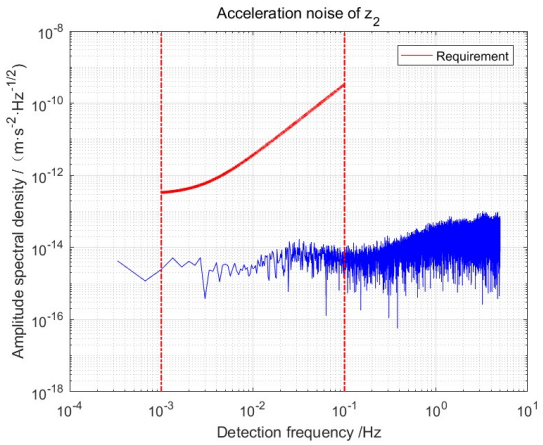

Fig. 11. Acceleration noise of the MRAC scheme in z_2 axis.

actuator loop. Then, a partial observation state feedback MRAC scheme is designed in this paper, to achieve the complex nonlinearity and noise suppression of the closed-loop system under incomplete and inaccurate state measurements. The numerical simulation verifies good closed-loop control performance and fault-tolerant effect. In future works, the rejection of acceleration noise from the external resources will be considered, and the fault-tolerant control scheme handling more complex fault with time-varying or fast changing rate will also be explored.

APPENDIX

The proof of **Theorem 4.2** is shown as follows. The Lyapunov function is obtained as:

$$V=\frac{1}{2}(\sum_{i=2}^{M}\tilde{\boldsymbol{\theta}}_{\boldsymbol{i}}{}^{\mathrm{T}}(t)\boldsymbol{\Gamma}_{\boldsymbol{\theta_i}}^{-1}\tilde{\boldsymbol{\theta}}_{\boldsymbol{i}}+tr[\tilde{\boldsymbol{\Psi}}^{\mathrm{T}}\boldsymbol{\Gamma}_{\boldsymbol{\Psi}}^{-1}\tilde{\boldsymbol{\Psi}}]+tr[\tilde{\boldsymbol{\Theta}}\boldsymbol{S}\tilde{\boldsymbol{\Theta}}^{\mathbf{T}}]). \tag{60}$$

Differentiate on both sides of (64) and denote:

$$\begin{aligned}\dot{V}=&-\sum_{i=2}^{M}\frac{\tilde{\boldsymbol{\theta}}_{\boldsymbol{i}}{}^{\mathrm{T}}\boldsymbol{\upsilon}_i(t)\boldsymbol{\eta}_{\boldsymbol{i}}(t)}{m^2(t)}-\frac{[h(s)[\hat{\boldsymbol{\omega}}]]^{\mathrm{T}}(t)\tilde{\boldsymbol{\Theta}}\boldsymbol{S}\boldsymbol{D}_{\boldsymbol{s}}\boldsymbol{\upsilon}(t)}{m^2(t)}\\&-\frac{\left[\left[\hat{\boldsymbol{\Theta}}^{\mathrm{T}}\right]h(s)[\hat{\boldsymbol{\omega}}]-h(s)\left[\hat{\boldsymbol{\Theta}}^{\mathrm{T}}\hat{\boldsymbol{\omega}}\right]\right]^{\mathrm{T}}\tilde{\boldsymbol{\Psi}}^{\mathrm{T}}\boldsymbol{\upsilon}(t)}{m^2(t)}\\=&-\frac{\boldsymbol{\upsilon}^{\mathrm{T}}(t)\boldsymbol{\upsilon}(t)}{m^2(t)}+[\boldsymbol{D}_{\boldsymbol{s}}\boldsymbol{S}h(s)[\boldsymbol{\varepsilon}_{\boldsymbol{u}}]]^{\mathrm{T}}(t)\upsilon(t)\\\leq&-\frac{\boldsymbol{\upsilon}^{\mathrm{T}}(t)\boldsymbol{\upsilon}(t)}{m^2(t)}+\gamma\boldsymbol{\upsilon}^{\mathrm{T}}(t)\boldsymbol{\upsilon}(t)\\&+\frac{\gamma^{-1}}{4}[\boldsymbol{D}_{\boldsymbol{s}}\boldsymbol{S}h(s)[\boldsymbol{\varepsilon}_{\boldsymbol{u}}]]^{\mathrm{T}}(t)\boldsymbol{D}_{\boldsymbol{s}}\boldsymbol{S}h(s)[\boldsymbol{\varepsilon}_{\boldsymbol{u}}](t)\\=&-\frac{1-m^2\gamma}{m^2}\boldsymbol{\upsilon}^{\mathrm{T}}(t)\boldsymbol{\upsilon}(t)\\&+\frac{\gamma^{-1}}{4}[\boldsymbol{D}_{\boldsymbol{s}}\boldsymbol{S}h(s)[\boldsymbol{\varepsilon}_{\boldsymbol{u}}]]^{\mathrm{T}}(t)\boldsymbol{D}_{\boldsymbol{s}}\boldsymbol{S}h(s)[\boldsymbol{\varepsilon}_{\boldsymbol{u}}](t).\end{aligned} \tag{61}$$

where γ is a parameter which is set to satisfy $\frac{1-m^2\gamma}{m^2}<0$. It can be proved that each adaptive estimation parameter $\boldsymbol{\theta_i}(t),\boldsymbol{\Theta}(t),\boldsymbol{\Psi}(t)$ is uniformly ultimately bounded, as the boundedness of $\dot{V}$ is ensured from (61),and $\dot{\boldsymbol{\theta}}_{\boldsymbol{i}}(t)\in L^2\cap L^\infty,\dot{\boldsymbol{\Theta}}(t)\in L^2\cap L^\infty,\dot{\boldsymbol{\Psi}}(t)\in L^2\cap L^\infty$, and $\boldsymbol{\upsilon}(t)/m(t)\in L^\infty$ are also obtained.

After getting the boundedness conclusion of parameters and closed-loop estimation errors, taking into account the influence of $\hat{\boldsymbol{y}}_{\boldsymbol{0}}(t)=\boldsymbol{C_0}\hat{\boldsymbol{x}}(t)$ on the convergence of other closed-loop signals and the tracking error of the system. Utilizing the output $\boldsymbol{y}(t)$ to represent $\hat{\boldsymbol{y}}_{\boldsymbol{0}}(t)=\boldsymbol{C_0}\hat{\boldsymbol{x}}(t)$, a set of filters is introduced as

$$sH_i(s)=1-K_i(s),K_i(s)=\frac{a_i^{d_m}}{(s+a_i)^{d_m}},i=1,2,3 \tag{62}$$

where $a_i>0$, which selection principle is sufficiently large and limited, d_m is the maximum dimension of $\boldsymbol{\xi_m}(s)$. This set of filters will be introduced to verify the boundness of closed-loop input, output and partial states based on controllable standard type and closed-loop sys-

This article has been accepted for publication in IEEE Transactions on Aerospace and Electronic Systems. This is the author's version which has not been fully edited and content may change prior to final publication. Citation information: DOI 10.1109/TAES.2023.3276342

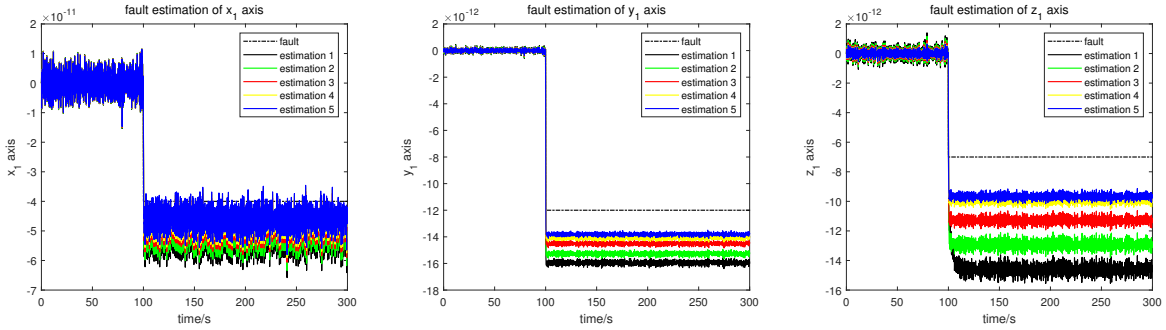

Fig. 12. Fault estimation by observer (15).

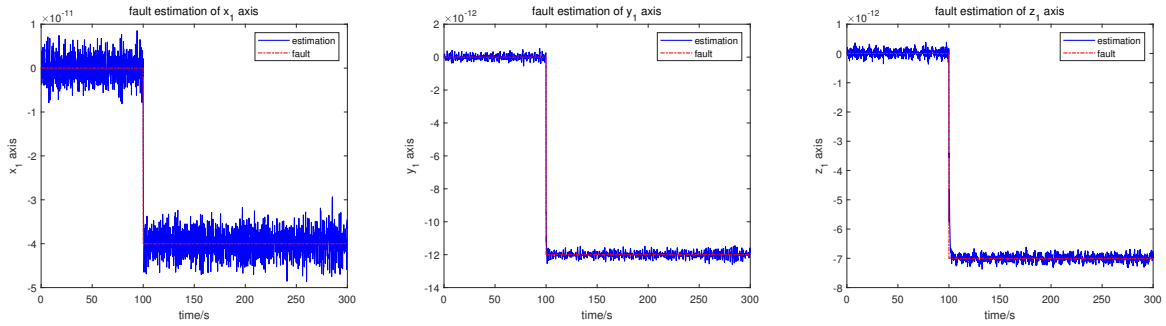

Fig. 13. Fault estimation by the proposed sequence Lyapunov scheme based observer.

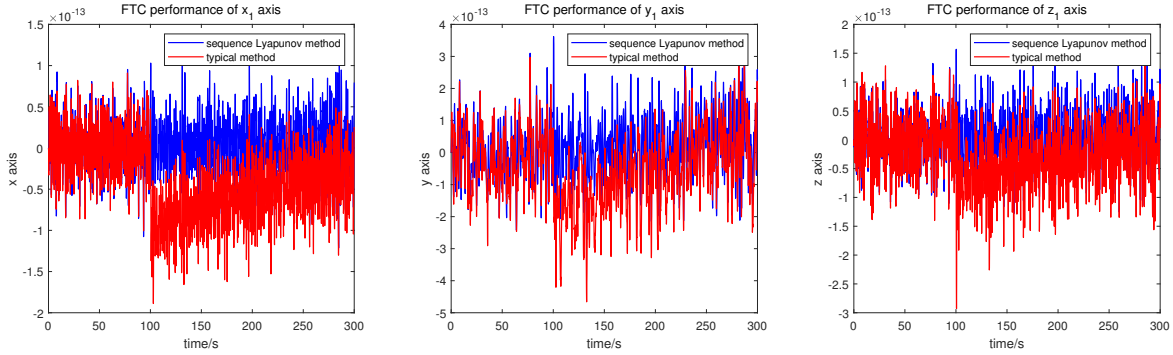

Fig. 14. Comparison of FTC performance.

tem characteristics. Express $h_i(t)$ as the impulse response function of the transfer function $H_i(s)$, according to [23], the L^1 operator norm form of $h_i(t)$ is given as follows:

$$\|h_i(\cdot)\|_1 = \int_0^\infty h_i(t)\,dt = \frac{d_m}{a_i}, a_i > 0, i = 1,2,3 \quad (63)$$

According to (65), for the bounded signal after shaping by filter $H_i(s)$, there exists $a_i^0 > 0$ to make the shape signal stable , for each finite $a_i > a_i^0$ denoting a finite gain.

Note the feedback controller given by (48), utilizing the full-state output, $\boldsymbol{\omega_1}(t) = \boldsymbol{F_1}(s)[\boldsymbol{u_T} + \boldsymbol{d_{TM}}](t) = \frac{\boldsymbol{A_1}(s)}{\Lambda(s)}[\boldsymbol{u_T} + \boldsymbol{d_{TM}}](t)$ is rewritten by $H_i(s), K_i(s)$ as:

$$\boldsymbol{F_1}(s)\boldsymbol{G^{-1}}(s)[\boldsymbol{y}](t) = {K_1}^{-1}(s)[\boldsymbol{\omega_1} - H_1(s)\,s[\boldsymbol{\omega_1}]](t) \quad (64)$$

To convert the partial observation output $\hat{\boldsymbol{y}}_{\boldsymbol{0}}(t)$ to the full state output $\boldsymbol{y}(t)$, according to the state expression given by the constant gain vector $\boldsymbol{L} \in \mathbb{R}^{n\times M}$ in the output matching, the nominal partial state $\boldsymbol{y_0}(t) = \boldsymbol{C_0 x}(t)$ is denoted as:

$$\boldsymbol{y_0}(t) = \boldsymbol{Q_1}(s)[\boldsymbol{u_T} + \boldsymbol{d_{TM}}](t) + \boldsymbol{Q_2}(s)[\boldsymbol{y}](t) \quad (65)$$

where, $\boldsymbol{Q_1}(s) = \boldsymbol{C_0}\frac{\boldsymbol{N_{01}}(s)}{\Lambda_0(s)}, \boldsymbol{Q_2}(s) = \boldsymbol{C_0}\frac{\boldsymbol{N_{02}}(s)}{\Lambda_0(s)}$ is stable, and $\boldsymbol{y_0}(t) \in L^\infty$ can be obtained.

Then the controller input analyzed. The controllable realization $(\boldsymbol{A_c}, \boldsymbol{B_c})$ of $\boldsymbol{\omega_1}(s) = \boldsymbol{F_1}(s)(\boldsymbol{u_T}(t) + \boldsymbol{d_{TM}})$ is expressed as:

$$\dot{\boldsymbol{\omega}}_{\boldsymbol{1}}(t) = \boldsymbol{A_c}\boldsymbol{\omega_1}(t) + \boldsymbol{B_c}(\boldsymbol{u_T}(t) + \boldsymbol{d_{TM}}) \quad (66)$$

Note that $\boldsymbol{A_c}$ is stable, shape (68) with the filter $H_i(s), K_i(s)$ and substitute the following partial observation state feedback, it can be obtained:

$$\hat{\boldsymbol{\omega}}_{\boldsymbol{2}}(t) = \boldsymbol{F_2}(s)[\hat{\boldsymbol{y}}_{\boldsymbol{0}}](t) = \frac{\boldsymbol{A_2}(s)}{\Lambda(s)}[\hat{\boldsymbol{y}}_{\boldsymbol{0}}](t)$$

$$\hat{\boldsymbol{y}}_{\boldsymbol{0}}(t) = \boldsymbol{Q_1}(s)[\boldsymbol{u_T} + \boldsymbol{d_{TM}}](t) + \boldsymbol{Q_2}(s)[\boldsymbol{y}](t) + \tilde{\boldsymbol{y}}_{\boldsymbol{0}}(t)$$

This article has been accepted for publication in IEEE Transactions on Aerospace and Electronic Systems. This is the author's version which has not been fully edited and content may change prior to final publication. Citation information: DOI 10.1109/TAES.2023.3276342

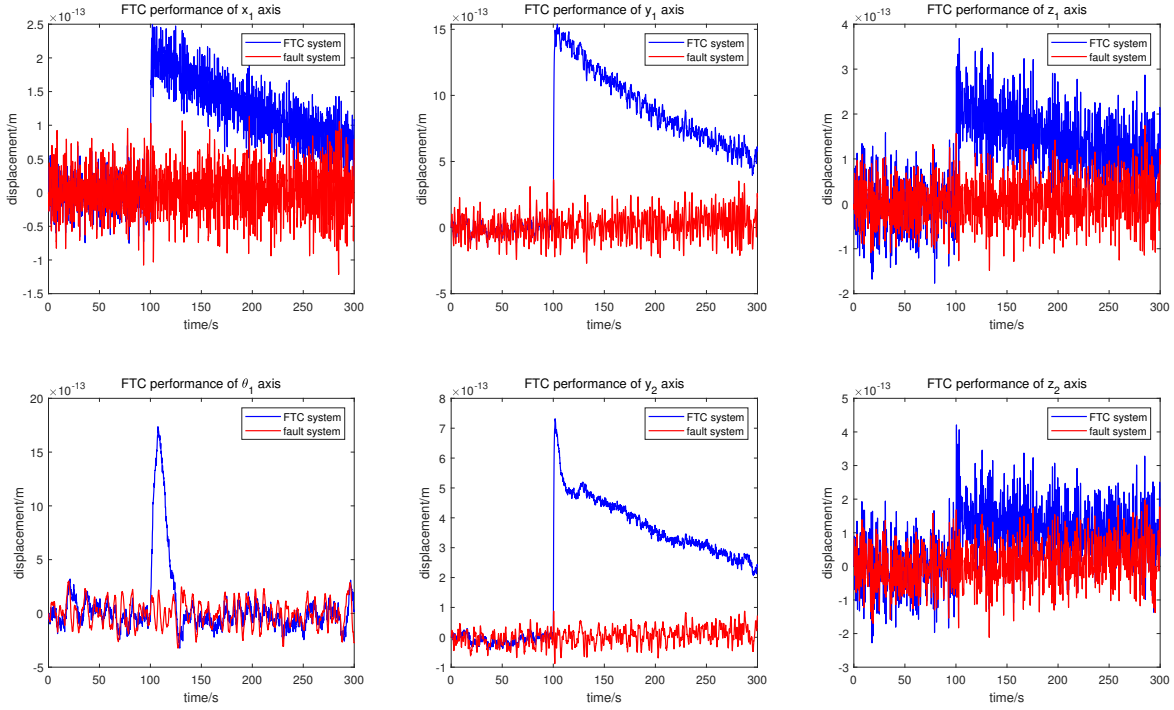

Fig. 15. FTC performance of the proposed sequence Lyapunov method in the drag-free axes.

Then $\boldsymbol{\omega_1}(t)$ is expressed as

$$\begin{aligned}\boldsymbol{\omega_1}(t) &= K_1(s)\boldsymbol{F_1}(s)\boldsymbol{G}^{-1}(s)[\boldsymbol{y}](t) + H_1(s)[\dot{\boldsymbol{\omega}}_1](t)\\ &= K_1(s)\boldsymbol{F_1}(s)\boldsymbol{G}^{-1}(s)[y](t) + H_1(s)[\boldsymbol{A_c}\boldsymbol{\omega_1}](t)\\ &+ H_1(s)\boldsymbol{B_c}[\boldsymbol{\Theta_1}^{\mathrm{T}}\boldsymbol{\omega_1} + \boldsymbol{\Theta_2}^{\mathrm{T}}\boldsymbol{F_2}(s)\boldsymbol{Q_1}(s)[\boldsymbol{u_T}+\boldsymbol{d_{TM}}]\\ &+ \boldsymbol{\Theta_2}^{\mathrm{T}}\boldsymbol{F_2}(s)\boldsymbol{Q_2}(s)[\boldsymbol{y}] + \boldsymbol{\Theta_2}^{\mathrm{T}}\boldsymbol{F_2}(s)[\tilde{\boldsymbol{y}}_0]\\ &+ \boldsymbol{\Theta_{20}}^{\mathrm{T}}\boldsymbol{Q_1}(s)[\boldsymbol{u_T}+\boldsymbol{d_{TM}}] + \boldsymbol{\Theta_{20}}^{\mathrm{T}}\boldsymbol{Q_2}(s)[\boldsymbol{y}]\\ &+ \boldsymbol{\Theta_{20}}^{\mathrm{T}}[\tilde{\boldsymbol{y}}_0] + \boldsymbol{\Theta_3}\boldsymbol{r} + \left(\boldsymbol{I}_M - \boldsymbol{\Theta_1}^{\mathrm{T}}\boldsymbol{F_1}\right)[\tilde{\boldsymbol{d}}_{\boldsymbol{TM}}]](t)\end{aligned} \tag{67}$$

Note that $\boldsymbol{\Theta_1}^{\mathrm{T}}$ is bounded, then $a_i^0 > 0$ so that the operator $\left(\boldsymbol{I} - H_1(s)\left(\boldsymbol{A_c} + \boldsymbol{B_c}\boldsymbol{\Theta_1}^{\mathrm{T}}(t)\right)\right)^{-1}$ shaped by $H_1(s)$ is stable, for any finite $a_i > a_i^0$ denoting finite gain. For $0 < a_1^0 < a_1$, organizing (69) as

$$\begin{aligned}\boldsymbol{\omega_1}(t) &= \boldsymbol{G_1}(s,\cdot)[\boldsymbol{u_T}+\boldsymbol{d_{TM}}](t) + \boldsymbol{G_2}(s,\cdot)[\boldsymbol{y}](t)\\ &+ \boldsymbol{G_3}(s,\cdot)[\boldsymbol{r}](t) + \boldsymbol{T_1}(s,t)[\left(\boldsymbol{\Theta_2}^{\mathrm{T}}\boldsymbol{F_2}(s) + \boldsymbol{\Theta_{20}}^{\mathrm{T}}\right)[\tilde{\boldsymbol{y}}_0]\\ &+ \left(\boldsymbol{I}_M - \boldsymbol{\Theta_1}^{\mathrm{T}}\boldsymbol{F_1}\right)[\tilde{\boldsymbol{d}}_{\boldsymbol{TM}}]](t)\end{aligned} \tag{68}$$

For $\boldsymbol{T_1}(s,t) \equiv \left(\boldsymbol{I} - H_1(s)\left(\boldsymbol{A_c} + \boldsymbol{B_c}\boldsymbol{\Theta_1}^{\mathrm{T}}(t)\right)\right)^{-1}$,

$$\begin{aligned}&\boldsymbol{G_1}(s,t) = \boldsymbol{T_1}(s,t)(H_1(s)\boldsymbol{B_c}\boldsymbol{\Theta_2}^{\mathrm{T}}(t)\boldsymbol{F_2}(s)\boldsymbol{Q_1}(s)\\ &+ H_1(s)\boldsymbol{B_c}\boldsymbol{\Theta_{20}}^{\mathrm{T}}(t)\boldsymbol{Q_1}(s)), \boldsymbol{G_2}(s,t) = \boldsymbol{T_1}(s,t)\\ &\times(K_1(s)\boldsymbol{F_1}(s)\boldsymbol{G}^{-1}(s) + H_1(s)\boldsymbol{B_c}\boldsymbol{\Theta_{20}}^{\mathrm{T}}(t)\boldsymbol{Q_2}(s)),\\ &\boldsymbol{G_3}(s,t) = \boldsymbol{T_1}(s,t)H_1(s)\boldsymbol{B_c}\boldsymbol{\Theta_3}^{\mathrm{T}}(t)\end{aligned}$$

are also stable operators with finite gain. Introducing the disturbance observation error into $\boldsymbol{\omega_1}(t)$, $\hat{\boldsymbol{\omega}}(t)$ is expressed as

$$\hat{\boldsymbol{\omega}}(t) = \left[\hat{\boldsymbol{\omega}}_1^{\mathrm{T}}(t), \hat{\boldsymbol{\omega}}_2^{\mathrm{T}}(t), \hat{\boldsymbol{y}}_0^{\mathrm{T}}(t), \boldsymbol{r}^{\mathrm{T}}(t)\right]^{\mathrm{T}} \tag{69}$$

where $\hat{\boldsymbol{\omega}}_1(t) = \boldsymbol{\omega_1}(t) + \tilde{\boldsymbol{\omega}}_1(t) = \boldsymbol{F_1}(s)[\boldsymbol{u_T} + \hat{\boldsymbol{d}}_{\boldsymbol{TM}}](t), \hat{\boldsymbol{\omega}}_2(t) = \boldsymbol{F_2}(s)[\hat{\boldsymbol{y}}_0](t)$. Then $\hat{\boldsymbol{\omega}}(t)$ is further rewritten as

$$\begin{aligned}\hat{\boldsymbol{\omega}}(t) &= \boldsymbol{G_4}(s,\cdot)[\boldsymbol{u_T}+\boldsymbol{d_{TM}}](t) + \boldsymbol{G_5}(s,\cdot)[\boldsymbol{y}](t)\\ &+ \boldsymbol{G_6}(s,\cdot)[\boldsymbol{r}](t) + \boldsymbol{D}\end{aligned} \tag{70}$$

where,

$$\begin{aligned}&\boldsymbol{G_4}(s,t) = [\boldsymbol{G_1}(s,t), \boldsymbol{F_1}(s)\boldsymbol{Q_1}(s), \boldsymbol{Q_1}(s), \boldsymbol{0}]^{\mathrm{T}},\\ &\boldsymbol{G_5}(s,t) = [\boldsymbol{G_2}(s,t), \boldsymbol{F_2}(s)\boldsymbol{Q_2}(s), \boldsymbol{Q_2}(s), \boldsymbol{0}]^{\mathrm{T}},\\ &\boldsymbol{G_6}(s,t) = [\boldsymbol{G_3}(s,t), \boldsymbol{0}, \boldsymbol{0}, \boldsymbol{I}]^{\mathrm{T}},\\ &\boldsymbol{D} = \boldsymbol{G_4}(s,t)[\tilde{\boldsymbol{d}}_{\boldsymbol{TM}}](t) + [\boldsymbol{T_1}(s,t)[\left(\boldsymbol{\Theta_2}^{\mathrm{T}}\boldsymbol{F_2}(s) + \boldsymbol{\Theta_{20}}^{\mathrm{T}}\right)\\ &\times[\tilde{\boldsymbol{y}}_0] + \left(\boldsymbol{I}_M - \boldsymbol{\Theta_1}^{\mathrm{T}}\boldsymbol{F_1}\right)[\tilde{\boldsymbol{d}}_{\boldsymbol{TM}}]](t), \boldsymbol{F_2}(s)[\tilde{\boldsymbol{y}}_0](t),\\ &[\tilde{\boldsymbol{y}}_0](t), \boldsymbol{0}]^{\mathrm{T}}\end{aligned}$$

Utilizing $\hat{\boldsymbol{\omega}}(t)$ to further establish the corresponding relationship between partial and full state output, and deducing the boundedness of $\boldsymbol{y}(t)$. Denote the first-order differential form of (60):

$$\dot{\boldsymbol{y}}(t) = \dot{\boldsymbol{y}}_{\boldsymbol{m}}(t) + s\boldsymbol{W_m}(s)\boldsymbol{\Theta_3^*}^{-1}[\tilde{\boldsymbol{\Theta}}^{\mathrm{T}}\hat{\omega} + \boldsymbol{\varepsilon_u}](t) \tag{71}$$

Multiply both sides of (73) by $H_2(s)$. Note that $sH_2(s) = 1 - K_2(s)$, rewrite (73) as

$$\begin{aligned}\boldsymbol{y}(t) &= \boldsymbol{K_2}(s)[\bar{\boldsymbol{y}}](t) + H_2(s)s\boldsymbol{W_m}(s)[\boldsymbol{r}](t)\\ &+ H_2(s)s\boldsymbol{W_m}(s)\boldsymbol{\Theta_3^*}^{-1}[\tilde{\boldsymbol{\Theta}}^{\mathrm{T}}[\boldsymbol{G_4}(s,\cdot)[\boldsymbol{u_T}+\boldsymbol{d_{TM}}\\ &+ \boldsymbol{G_5}(s,\cdot)[\boldsymbol{y}] + \boldsymbol{G_6}(s,\cdot)[\boldsymbol{r}] + \boldsymbol{D} + \boldsymbol{\varepsilon_u}](t)\end{aligned} \tag{72}$$

Similar to $\boldsymbol{T_1}(s,t)$, $(\boldsymbol{I} - H_2(s)s\boldsymbol{W_m}(s)\boldsymbol{\Theta_3^*}^{-1}\tilde{\boldsymbol{\Theta}}^{\mathrm{T}} \times \boldsymbol{G_5}(s,t))^{-1}$ is also considered as a stable operator. For

any finite $a_2 > a_2^0$, there exists $a_2^0 > 0$. For $0 < a_2^0 < a_2$, it can be denoted

$$\begin{aligned}\boldsymbol{y}(t) &= \boldsymbol{G_7}(s,\cdot)[\boldsymbol{u_T}+\boldsymbol{d_{TM}}](t)+\boldsymbol{G_8}(s,\cdot)[\bar{\boldsymbol{y}}](t)\\ &+\boldsymbol{G_9}(s,\cdot)[\boldsymbol{r}](t)+\boldsymbol{D_1}\end{aligned} \tag{73}$$

where, for $\boldsymbol{T_2}(s,t) = (\boldsymbol{I}-\boldsymbol{H_2}(s)s\boldsymbol{W_m}(s)\boldsymbol{\Theta_3^{*-1}}\tilde{\boldsymbol{\Theta}}^{\mathrm{T}}\boldsymbol{G_5})^{-1}$,

$$\boldsymbol{G_7}(s,t) = \boldsymbol{T_2}(s,t)H_2(s)s\boldsymbol{W_m}(s)\boldsymbol{\Theta_3^{*-1}}\tilde{\boldsymbol{\Theta}}^{\mathrm{T}}\boldsymbol{G_4}(s,\cdot)$$

$$\boldsymbol{G_8}(s,t) = \boldsymbol{T_2}(s,t)K_2(s)h^{-1}(s)$$

$$\boldsymbol{G_9}(s,t) = \boldsymbol{T_2}(s,t)H_2(s)s\boldsymbol{W_m}(s)\left(\boldsymbol{I}+\boldsymbol{\Theta_3^{*-1}}\tilde{\boldsymbol{\Theta}}^{\mathrm{T}}\boldsymbol{G_6}\right)$$

$$\boldsymbol{D_1} = \boldsymbol{T_2}(s,t)H_2(s)s\boldsymbol{W_m}(s)\boldsymbol{\Theta_3^{*-1}}\left[\tilde{\boldsymbol{\Theta}}^{\mathrm{T}}\boldsymbol{D}+\boldsymbol{\varepsilon_u}\right](t)$$

is a stable operator with finite gain, and denote $\boldsymbol{y}(t) \in L^\infty$, which is utilized to derive the boundness of $\hat{\boldsymbol{\omega}}(t)$. Organize $\hat{\boldsymbol{\omega}}(t)$ as

$$\begin{aligned}\hat{\boldsymbol{\omega}}(t) &= (\boldsymbol{G_4}(s,\cdot)+\boldsymbol{G_5}(s,\cdot)\boldsymbol{G_7}(s,\cdot))[\boldsymbol{u_T}+\boldsymbol{d_{TM}}](t)\\ &+\boldsymbol{G_5}(s,\cdot)\boldsymbol{G_8}(s,\cdot)[\bar{\boldsymbol{y}}](t)+\boldsymbol{G_5}(s,\cdot)\boldsymbol{D_1}+\boldsymbol{D}\\ &+(\boldsymbol{G_6}(s,\cdot)+\boldsymbol{G_5}(s,\cdot)\boldsymbol{G_9}(s,\cdot))[\boldsymbol{r}](t)\end{aligned} \tag{74}$$

Then it is obtained $\hat{\boldsymbol{\omega}}(t) \in L^\infty$.

Introduce (76) into $\boldsymbol{u_T}(t)$ to deduce its boundedness:

$$\begin{aligned}\boldsymbol{u_T} &= \boldsymbol{G_{10}}(s,\cdot)\hat{\boldsymbol{\Theta}}^{\mathrm{T}}(t)\boldsymbol{G_5}(s,\cdot)\boldsymbol{G_8}(s,\cdot)[\bar{\boldsymbol{y}}](t)\\ &+\boldsymbol{G_{10}}(s,\cdot)\hat{\boldsymbol{\Theta}}^{\mathrm{T}}(t)(\boldsymbol{G_6}(s,\cdot)+\boldsymbol{G_5}(s,\cdot)\boldsymbol{G_9}(s,\cdot))[\boldsymbol{r}](t)\\ &+\boldsymbol{G_{10}}(s,\cdot)(\hat{\boldsymbol{\Theta}}^{\mathrm{T}}(t)(\boldsymbol{G_5}(s,\cdot)\boldsymbol{D_1}+\boldsymbol{D})+\hat{\boldsymbol{\Theta}}^{\mathrm{T}}(t)\\ &\times(\boldsymbol{G_4}(s,\cdot)+\boldsymbol{G_5}(s,\cdot)\boldsymbol{G_7}(s,\cdot))\tilde{\boldsymbol{d}}_{\boldsymbol{TM}}-\hat{\boldsymbol{d}}_{\boldsymbol{TM}}(t)\end{aligned} \tag{75}$$

where $\boldsymbol{G_{10}}(s,t) = (\boldsymbol{I}_M - \hat{\boldsymbol{\Theta}}^T(t)(\boldsymbol{G_4}+\boldsymbol{G_5}\boldsymbol{G_7}))^{-1}$ is a stable operator with finite gain. Then $\boldsymbol{u_T}(t) \in L^\infty$ is obtained. Review the output expression of the closed-loop system with the introduction of shaper $h(s)$:

$$\bar{\boldsymbol{y}}(t) = \bar{\boldsymbol{y}}_{\boldsymbol{m}}(t)+\boldsymbol{W_m}(s)\left[\boldsymbol{\upsilon}-\boldsymbol{\sigma}-\hat{\boldsymbol{\Psi}}\boldsymbol{\xi}\right](t) \tag{76}$$

where,

$$\boldsymbol{\sigma} = \left[\boldsymbol{0}, \hat{\boldsymbol{\theta}}_{\boldsymbol{2}}^{\mathrm{T}}\boldsymbol{\eta_2}(t), \hat{\boldsymbol{\theta}}_{\boldsymbol{3}}^{\mathrm{T}}\boldsymbol{\eta_3}(t), ..., \hat{\boldsymbol{\theta}}_{\boldsymbol{M}}{}^{\mathrm{T}}\boldsymbol{\eta_M}(t)\right]^{\mathrm{T}}$$

$$\boldsymbol{\xi}(t) = \hat{\boldsymbol{\Theta}}^{\mathrm{T}}(t)h(s)[\hat{\boldsymbol{\omega}}](t)-h(s)\left[\hat{\boldsymbol{\Theta}}^{\mathrm{T}}\hat{\boldsymbol{\omega}}\right](t)$$

$$\bar{\boldsymbol{y}}_{\boldsymbol{m}}(t) = h(s)[\boldsymbol{y_m}](t)$$

According to

$$\begin{aligned}&\boldsymbol{\xi}(t) = [\boldsymbol{\xi_1}(t), \ldots, \boldsymbol{\xi_M}(t)]^{\mathrm{T}},\\ &\boldsymbol{\Theta}(t) = \left[\bar{\boldsymbol{\theta}}_{\boldsymbol{1}}{}^{\mathrm{T}}(t), \ldots, \bar{\boldsymbol{\theta}}_{\boldsymbol{M}}{}^{\mathrm{T}}(t)\right]^{\mathrm{T}},\\ &f(s) = s^{d_m}+\hat{a}_{dm}s^{d_m-1}+\cdots+\hat{a}_1 s+\hat{a}_0\end{aligned}$$

Expanding the i-th column of $\xi(t)$ as follows:

$$\begin{aligned}\boldsymbol{\xi_i}(t) &= \frac{s^{d_m-1}+\hat{a}_{d_m-1}s^{d_m-2}+\cdots+\hat{a}_1}{f(s)}\left[\dot{\hat{\boldsymbol{\theta}}}_{\boldsymbol{i}}{}^{\mathrm{T}}\frac{[\hat{\boldsymbol{\omega}}]}{f(s)}\right](t)\\ &+\frac{s^{d_m-2}+\hat{a}_{d_m-1}s^{d_m-2}+\cdots+\hat{a}_2}{f(s)}\left[\dot{\hat{\boldsymbol{\theta}}}_{\boldsymbol{i}}{}^{\mathrm{T}}\frac{s}{f(s)}[\hat{\boldsymbol{\omega}}]\right](t)\\ &+\cdots\frac{1}{f(s)}\left[\dot{\hat{\boldsymbol{\theta}}}_{\boldsymbol{i}}{}^{\mathrm{T}}\frac{s^{d_m-1}}{f(s)}[\hat{\boldsymbol{\omega}}]\right](t)\end{aligned} \tag{77}$$

Then the boundedness of $\xi(t)$ can be denoted. According to (75) and (78), $\|\bar{\boldsymbol{y}}(t)\|$ is expressed as

$$\|\bar{\boldsymbol{y}}(t)\| \le \|\boldsymbol{T_3}(s,\cdot)\varsigma_1\boldsymbol{T_4}(s,\cdot)\|\|\bar{\boldsymbol{y}}\|+\varsigma_0+h(s)\|\boldsymbol{D_1}\| \tag{78}$$

For some $\varsigma_0(t) \in L^\infty$, $h(s)\|\boldsymbol{D_1}\| \in L^\infty$,$\varsigma_1(t) \in L^\infty \cap L^2 \ge 0$. Similar to the operator $\boldsymbol{T_1}(s,t)$, some operator $\boldsymbol{T_3}(s,t), \boldsymbol{T_4}(s,t)$ are strictly stable, and the operator $\boldsymbol{T_4}(s,t)$ has a non-negative impulse response function. According to [22], it is known that $\bar{\boldsymbol{y}}(t)$ is bounded.

After the above-mentioned closed-loop signal has been proved to be bounded, the convergence of the output tracking is derived. For $\bar{\boldsymbol{e}}(t) = \boldsymbol{\xi_m}(s)h(s)[\boldsymbol{e}](t)$, it is obtained

$$\begin{aligned}\boldsymbol{e}(t) &= \boldsymbol{W_m}(s)\boldsymbol{\Theta_3^{*-1}}\left[\tilde{\boldsymbol{\Theta}}^{\mathrm{T}}\boldsymbol{\omega}+\boldsymbol{\varepsilon_u}\right](t)\\ &= H_3(s)s\boldsymbol{W_m}(s)\boldsymbol{\Theta_3^{*-1}}\left[\tilde{\boldsymbol{\Theta}}^{\mathrm{T}}\boldsymbol{\omega}+\boldsymbol{\varepsilon_u}\right](t)\\ &+\boldsymbol{W_m}(s)K_3(s)h^{-1}(s)[\bar{\boldsymbol{e}}](t)\end{aligned} \tag{79}$$

According to

$$\begin{aligned}&\lim_{t\to\infty}\sup\left\|\boldsymbol{W_m}(s)K_3(s)h^{-1}(s)[\bar{\boldsymbol{e}}](t)\right\|\\ &=\lim_{t\to\infty}\sup\|\boldsymbol{W_m}(s)K_3(s)\boldsymbol{D_s}\boldsymbol{S}[\boldsymbol{\varepsilon_u}](t)\|\\ &\le\|\boldsymbol{W_m}(s)K_3(s)\boldsymbol{D_s}\boldsymbol{S}(\rho_d+\|\boldsymbol{K_1^*}\|\rho_x)\|\end{aligned} \tag{80}$$

Then the filter parameters $a_3 > 0$ in the filter $K_3(s)$ are finite, it is determined that

$$s\boldsymbol{W_m}(s)\boldsymbol{\Theta_3^{*-1}}\left[\tilde{\boldsymbol{\Theta}}^{\mathrm{T}}\boldsymbol{\omega}+\boldsymbol{\varepsilon_u}\right](t) \in L^\infty,$$

yields

$$\begin{aligned}&\lim_{t\to\infty}\sup\|\boldsymbol{e}(t)\| \le c_3\frac{d_m}{a_3}\\ &+\|\boldsymbol{W_m}(s)K_3(s)\boldsymbol{D_s}\boldsymbol{S}(\rho_d+\|\boldsymbol{K_1^*}\|\rho_x)\|\end{aligned}$$

where c_3, d_m are constants. Considering a_3 can take any large value, the steady-state accuracy of $\|\boldsymbol{e}(t)\|$ can be obtained as

$$\limsup_{t\to\infty}\|\boldsymbol{e}(t)\| \le \|\boldsymbol{W_m}(s)K_3(s)\boldsymbol{D_s}\boldsymbol{S}(\rho_d+\|\boldsymbol{K_1^*}\|\rho_x)\|$$

When the system has actuator faults, the designed reconfiguration controller is introduced to compensate the actuator bias. The part of compensation effect will produce a bounded estimation error ρ_r. Therefore, the nominal system input error $\boldsymbol{\varepsilon_u}$ is corrected as follows:

$$\boldsymbol{\varepsilon_{u_c}}(t) = \tilde{\boldsymbol{d}}_{\boldsymbol{TM}}+\boldsymbol{K_1}^{*\mathrm{T}}\tilde{\boldsymbol{x}}(t)+\tilde{\tilde{\boldsymbol{u}}} \tag{81}$$

Therefore, in the fault-tolerant system, the tracking error accuracy $\boldsymbol{e_c}(t)$ is corrected to:

$$\begin{aligned}&\lim_{t\to\infty}\sup\|\boldsymbol{e_c}(t)\| \le |\boldsymbol{W_m}(s)K_3(s)\boldsymbol{D_s}\boldsymbol{S}\\ &\times(\rho_d+\rho_r+\|\boldsymbol{K_1^*}\|\rho_x)\|\end{aligned}$$

Since the actuator fault compensation error $\tilde{\tilde{\boldsymbol{u}}}$ is continuously bounded, it can be denoted that when the system has actuator faults, the closed-loop tracking error $\boldsymbol{e_c}(t)$ is still continuously bounded, and the upper bound of the L^2 vector norm is not greater than $\|\boldsymbol{W_m}(s)K_3(s)\boldsymbol{D_s}\boldsymbol{S}(\rho_d+\rho_r+\|\boldsymbol{K_1^*}\|\rho_x)\|$. ∇

REFERENCES

[1] W. Fichter, P. Gath, S. Vitale and et al., "LISA Pathfinder Drag-free Control and System Implications," *Classical and Quantum Gravity*, vol. 22, no.10, pp. S139, 2005.

[2] X. Lian and et al., "Frequency Separation Control for Drag free Satellite With Frequency Domain Constraints," *IEEE Transactions on Aerospace and Electronic Systems*, vol. 57, no. 6, pp. 4085-4096, Dec. 2021, https://doi.org/10.1109/TAES.2021.3088456.

[3] S. Wu and D. Fertin, "Spacecraft Drag-free Attitude Control System Design with Quantitative Feedback Theory," *Acta Astronautica*, vol.62, no.12, pp. 668-682, 2008.

[4] F. Mobley, G. Fountain, A. Sadilek, P. Worden and R. Patten, "Electromagnetic Suspension for the Tip-II Satellite," *IEEE Transactions on Magnetics*., vol. 11, no. 6, pp. 1712-1716, November 1975, https://doi.org/10.1109/TMAG.1975.1058972.

[5] E. Canuto, A. Molano and L. Massotti, "Drag-Free Control of the GOCE Satellite: Noise and Observer Design," *IEEE Transactions on Control Systems Technology*, vol. 18, no. 2, pp. 501-509, March 2010, https://doi.org/10.1109/TCST.2009.2020169.

[6] S. Wu and et al., "Attitude Control of LISA Pathfinder Spacecraft with Micro-Newton FEEP Thrusters under Multiple Failures," *AIAA Guidance, Navigation, and Control Conference*, 2010.

[7] S. Wu and et al., "Attitude Stabilization of LISA Pathfinder Spacecraft Using Colloidal Micro-Newton Thrusters," *AIAA Guidance, Navigation, and Control Conference*, 2011.

[8] S. Zhu, D. Wang, Q. Shen and E. Poh, "Satellite Attitude Stabilization Control with Actuator Faults," *Journal of Guidance, Control, and Dynamics*, vol. 40, no. 5, pp. 1304-1313, 2017.

[9] E. Canuto, "Drag-free and Attitude Control for the GOCE Satellite," *Automatica*, vol. 44, no. 7, pp. 1766-1780, 2008.

[10] Q. Shen, C. F. Yue, C. H. Goh, B. L. Wu and D. W. Wang, "Rigid-Body Attitude Tracking Control Under Actuator Faults and Angular Velocity Constraints," *IEEE/ASME Transactions on Mechatronics*, vol. 23, no. 3, pp. 1338-1349, June 2018, https://doi.org/10.1109/TMECH.2018.2812871.

[11] Q. Hu, X. Shao and W. Chen, "Robust Fault-Tolerant Tracking Control for Spacecraft Proximity Operations Using Time-Varying Sliding Mode," *IEEE Transactions on Aerospace and Electronic Systems*, vol. 54, no. 1, pp. 2-17, Feb. 2018, https://doi.org/10.1109/TAES.2017.2729978.

[12] Q. Shen, C. Yue, C. H. Goh and D. Wang, "Active Fault-Tolerant Control System Design for Spacecraft Attitude Maneuvers with Actuator Saturation and Faults," *IEEE Transactions on Industrial Electronics*, vol. 66, no. 5, pp. 3763-3772, May 2019, https://doi.org/10.1109/TIE.2018.2854602.

[13] Q. Shen, C. Yue, X. Yu and C. H. Goh,"Fault Modeling, Estimation, and Fault-Tolerant Steering Logic Design for Single-Gimbal Control Moment Gyro," *IEEE Transactions on Control Systems Technology*, vol. 29, no. 1, pp. 428-435, Jan. 2021, https://doi.org/doi:10.1109/TCST.2020.2971959.

[14] B. Li, Q. Hu, G. Ma and Y. Yang, "Fault-Tolerant Attitude Stabilization Incorporating Closed-Loop Control Allocation Under Actuator Failure," *IEEE Transactions on Aerospace and Electronic Systems*, vol. 55, no. 4, pp. 1989-2000, Aug. 2019, https://doi.org/10.1109/TAES.2018.2880035.

[15] H. Gui,"Observer-Based Fault-Tolerant Spacecraft Attitude Tracking Using Sequential Lyapunov Analyses," *IEEE Transactions on Automatic Control*, vol. 66, no. 12, pp. 6108-6114, Dec. 2021, https://doi.org/doi:10.1109/TAC.2021.3062159.

[16] P. McNamara and et al., "LISA Pathfinder", *Classical and Quantum Gravity*, vol. 63, no. 1, pp. 283-290, 2017.

[17] W. Fichter, A. Schleicher, S. Bennani and S. Wu., "Closed Loop Performance and Limitations of the LISA Pathfinder Drag-free Control System," *AIAA Guidance, Navigation and Control Conference and Exhibit*, pp. 6732, 2007.

[18] G. Luisella, T. Fenal, and S. Wu, "Attitude and Orbit Control Systems for the LISA Pathfinder Mission," *Aerospace Science and Technology*, vol. 24, no. 1, pp. 283-294, 2013.

[19] A. Einstein and R. Nathan, "On Gravitational Waves," *Journal of the Franklin Institute*, vol. 223, no. 1, pp. 43-54, 1937.

[20] Q. Shen, D. Wang, S. Zhu and K. Poh, "Finite-Time Fault-Tolerant Attitude Stabilization for Spacecraft with Actuator Saturation," *IEEE Transactions on Aerospace and Electronic Systems*, vol. 51, no. 3, pp. 2390-2405, July 2015, https://doi.org/10.1109/TAES.2015.130725.

[21] B. Li, Q. Hu, Y. Yu and G. Ma, "Observer-Based Fault-Tolerant Attitude Control for Rigid Spacecraft," *IEEE Transactions on Aerospace and Electronic Systems*., vol. 53, no. 5, pp. 2572-2582, Oct. 2017, https://doi.org/10.1109/TAES.2017.2705318.

[22] S. Ge, and G. Tao, "Partial-State Feedback Multivariable MRAC and Reduced-Order Designs," *Automatica*, vol. 129, pp. 109622, 2021.

[23] S. B. Roy, S. Bhasin and I. N. Kar, "Combined MRAC for Unknown MIMO LTI Systems With Parameter Convergence," *IEEE Transactions on Automatic Control*, vol. 63, no. 1, pp. 283-290, Jan. 2018, https://doi.org/10.1109/TAC.2017.2725955.

[24] J. Guo,G. Tao, and Y. Liu, "A Multivariable MRAC Scheme with Application to a Nonlinear Aircraft Model," *Automatica*, vol. 47, no. 4, pp. 804-812, 2018.

[25] L. Sun, W. Huo and Z. Jiao, "Disturbance-Observer-Based Robust Relative Pose Control for Spacecraft Rendezvous and Proximity Operations Under Input Saturation," *IEEE Transactions on Aerospace and Electronic Systems*, vol. 54, no. 4, pp. 1605-1617, Aug. 2018, https://doi.org/10.1109/TAES.2018.2798239.

[26] J. Qiu, T. Wang, K. Sun, I. J. Rudas and H. Gao, "Disturbance Observer-Based Adaptive Fuzzy Control for Strict-Feedback Nonlinear Systems With Finite-Time Prescribed Performance," *IEEE Transactions on Fuzzy Systems*, vol. 30, no. 4, pp. 1175-1184, April 2022, https://doi.org/10.1109/TFUZZ.2021.3053327.

[27] Y. Jiang, D. Shi, J. Fan, T. Chai and T. Chen, "Event-Triggered Model Reference Adaptive Control for Linear Partially Time-Variant Continuous-Time Systems with Nonlinear Parametric Uncertainty," *IEEE Transactions on Automatic Control* https://doi.org/10.1109/TAC.2022.3169847.